A set of functionally-defined brain regions with improved representation of the subcortex and cerebellum

Benjamin A. Seitzman[1]*, BS, seitzman@wustl.edu

Caterina Gratton[1], PhD, cgratton@wustl.edu

Scott Marek[1], PhD, smarek@wustl.edu

Ryan V. Raut[3], BS, raut@wustl.edu

Nico U.F. Dosenbach[1,3,4,6,7], MD, PhD, dosenbachn@wustl.edu

Bradley L. Schlaggar[1,2,3,4,5], MD, PhD, schlaggarb@wustl.edu

Steven E. Petersen[1,8,3,5], PhD, sep@wustl.edu

Deanna J. Greene[2,3], PhD, dgreene@wustl.edu

Departments of [1]Neurology, [2]Psychiatry, [3]Radiology, [4]Pediatrics, [5]Neuroscience, [6]Occupational Therapy, Washington University in St. Louis- School of Medicine, 660 S Euclid Ave, St. Louis, MO 63110, USA
[7]Department of Biomedical Engineering, Washington University in St. Louis- School of Engineering and Applied Science, One Brookings Dr, St. Louis, MO 63130, USA
[8]Department of Psychological and Brain Sciences, Washington University in St. Louis, One Brookings Dr, St. Louis, MO 63130, USA

*Corresponding Author: Benjamin A. Seitzman
Washington University in St. Louis, Department of Neurology
4525 Scott Ave, Box 8111
St. Louis, MO 63110, USA
seitzman@wustl.edu
Phone: +1 314 362 4155
Fax: 314 362 2186

Abstract

An important aspect of network-based analysis is robust node definition. This issue is critical for functional brain network analyses, as poor node choice can lead to spurious findings and misleading inferences about functional brain organization. Two sets of functional brain nodes from our group are well represented in the literature: (1) 264 volumetric regions of interest (ROIs) reported in Power et al., 2011 and (2) 333 surface parcels reported in Gordon et al., 2016. However, subcortical and cerebellar structures are either incompletely captured or missing from these ROI sets. Therefore, properties of functional network organization involving the subcortex and cerebellum may be underappreciated thus far. Here, we apply a winner-take-all partitioning method to resting-state fMRI data and careful consideration of anatomy to generate novel functionally-constrained ROIs in the thalamus, basal ganglia, amygdala, hippocampus, and cerebellum. We validate these ROIs in three datasets via several anatomical and functional criteria, including known anatomical divisions and functions, as well as agreement with existing literature. Further, we demonstrate that combining these ROIs with established cortical ROIs recapitulates and extends previously described functional network organization. This new set of ROIs is made publicly available for general use, including a full list of MNI coordinates and functional network labels.

Keywords: subcortex, cerebellum, networks, resting-state, functional connectivity

1. Introduction

The brain is organized into areas that interact with one another to form distributed large-scale networks (Allman and Kaas, 1971; Felleman and Van Essen, 1991; Petersen and Sporns, 2015). Researchers studying the brain at the network level have revealed both basic principles of brain organization (Bassett and Bullmore, 2006; Honey et al., 2007; Power et al., 2011; Sporns et al., 2004; van den Heuvel and Sporns, 2011; Yeo et al., 2011) and insights into neurologic and psychiatric diseases (Corbetta and Shulman, 2011; Kim et al., 2014; Seeley et al., 2009; Sorg et al., 2007). Much of this work has borrowed concepts and tools from the field of graph theory in order to model the brain as a network (Bullmore and Sporns, 2009; Sporns, 2011). A graph is a mathematical description of a network, which is composed of a set of elements (nodes) and their pairwise relationships (edges (Bondy and Murty, 1976)). Therefore, any network approach requires the definition of a set of nodes, such as regions of interest (ROIs) in the case of brain networks.

Ideally, nodes should be internally coherent (e.g., functionally homogeneous) and independent, separable units (Bullmore and Bassett, 2011; Butts, 2009, 2008). Brain areas and their constituent components—local circuits, columns, and domains (Kaas, 2012)—display many of these properties, and thus, are suitable nodes for brain network analysis. Research efforts focused on node definition often employ data-driven techniques to parcellate the cerebral cortex into a set of ROIs meant to represent putative brain areas (Cohen et al., 2008; Craddock et al., 2012; Glasser et al., 2016; Gordon et al., 2016; Nelson et al., 2010; Power et al., 2011; Schaefer et al., 2017; Wig et al., 2013). Most such studies have used resting-state functional connectivity MRI, which measures correlations in low-frequency blood-oxygen-level-dependent signals across the whole brain while subjects remain awake and alert without engaging in an explicit task (Biswal et al., 1995; Gusnard and Raichle, 2001; Snyder and Raichle, 2012). While many of these existing sets of ROIs sample the cortex quite well, most approaches have under-sampled or completely omitted the subcortex and cerebellum.

The poorer representation of these structures is a limitation of previous work, as the subcortex and cerebellum are known to be integral for many behavioral, cognitive, and affective functions. For example, regions of the cerebellum are involved in adaptive behaviors (Thach et al., 1992), including fast adaptations, like eye-blink conditioning (Steinmetz et al., 1992; Perrett et al., 1993), as well as those that occur over longer timescales, like prism adaptation (Martin et al., 1996; Baizer et al., 1999; Morton and Bastian, 2004), and higher order cognitive functions, such as semantic processing (Fiez, 2016). Likewise, regions of the basal ganglia and thalamus are important for both lower level sensory and higher order cognitive functions (Alexander et al., 1986; Jones, 1985). Furthermore, subcortical structures and the cerebellum have been implicated in a variety of neurologic and psychiatric diseases. For instance, the basal ganglia are affected in several movement disorders (Greene et al., 2017, 2013; Rajput, 1993; Vonsattel et al., 1985), the hippocampus is disrupted in Alzheimer Disease (Hardy and Selkoe, 2002), the amygdala is implicated in Urbach-Wiethe Disease (Siebert et al., 2003), and the cerebellum is disturbed in Schizophrenia (Andreasen et al., 1996;

Bigelow et al., 2006; Brown et al., 2005; Kim et al., 2014) and Autism Spectrum Disorder (Fatemi et al., 2002), to name a few. Moreover, interactions between the cortex and both subcortical and cerebellar regions are crucial for carrying out functions in health (Bostan and Strick, 2018; Greene et al., 2014; Hwang et al., 2017; Kiritani et al., 2012) and disease (Andreasen et al., 1999; Gratton et al., 2018a; Schmahmann, 2004). Because of these interactions between multiple structures, it has been postulated that subcortical regions may have important hub-like properties for integrating brain systems (Hwang et al., 2017). Thus, brain network analyses should include these important regions in order to have a more complete picture of brain organization and function.

An issue potentially impeding the inclusion of these regions is that subcortical and deep cerebellar nuclei are small relative to the spatial resolution of fMRI, often occupying just a few voxels, whereas brain areas in the cerebral cortex (e.g. Area V1) are often larger. Furthermore, depending on the acquisition sequence, these regions may have lower signal quality (Ojemann et al., 1997) or, especially for the cerebellum, may be captured incompletely. Finally, most existing techniques for parcellating the brain into areas, such as the one used by Gordon and colleagues (2016), were designed for the cortical surface, making them less easily applied to structures where surface-based mapping is less appropriate (basal ganglia, thalamus), prone to error (medial temporal lobe) (Wisse et al., 2014), or less well-established (cerebellum). Despite these difficulties, including the subcortex and cerebellum is necessary to have a full representation of the whole brain as a network.

Our lab previously published two (now widely used) sets of ROIs: (1) 264 volumetric ROIs (Power et al., 2011) and (2) 333 surface-based cortical parcels (Gordon et al., 2016). The first was created via combined task fMRI meta-analysis and resting-state functional correlation mapping, and the second was created via a gradient-based parcellation of resting-state fMRI data. These two ROI sets sample the cortex well, representing a diverse set of brain areas that can be organized into functional networks. Many investigators have used them to describe functional brain organization in a variety of healthy samples (Power et al., 2013; Zanto and Gazzaley, 2013), lifespan cohorts (Baniqued et al., 2018; Gallen et al., 2016; Gu et al., 2015; Nielsen et al., 2018; Rudolph et al., 2017), as well as populations with neurologic and psychiatric diseases (Gratton et al., 2018a; Greene et al., 2017; Sheffield et al., 2015; Siegel et al., 2018). However, the first set (264 volumetric ROIs) under-samples subcortical and cerebellar structures, as only 17 ROIs are non-cortical, and the second set (333 parcels) is restricted to the cortex only, which is true of other popular ROI sets, e.g. (Glasser et al., 2016; Yeo et al., 2011).

The goal of the current study was to expand these ROI sets to better represent subcortical and cerebellar structures. Novel ROIs were created in the thalamus, basal ganglia, and cerebellum by use of a data-driven, winner-take-all partitioning technique that operates on resting-state fMRI data (Choi et al., 2012; Greene et al., 2014; Zhang et al., 2010). Additional ROIs were generated in the amygdala and hippocampus on the basis of anatomical sub-divisions and previously published literature. The ROIs were

validated via anatomical and functional criteria. Finally, we described whole-brain functional network organization using these refined subcortical and cerebellar ROIs combined with previously established cortical ROIs. The fully updated set of ROIs is made publicly available for general use, including a list of coordinates and consensus functional network labels, at https://greenelab.wustl.edu/data_software.

2. Material and Methods

2.1. Primary dataset- WashU 120

2.1.1. Dataset characteristics

The primary dataset used in this study has been described previously (Power et al., 2011). Eyes-open resting-state fMRI data were acquired from 120 healthy, right-handed, native English speaking, young adults (60 F, age range 18-32, mean age 24.7). Subjects were recruited from the Washington University community and screened with a self-report questionnaire. Exclusion criteria included no current or previous history of neurologic or psychiatric diagnosis as well as no head injuries resulting in a loss of consciousness for more than 5 minutes. Informed consent was obtained from all participants, and the Washington University Internal Review Board approved the study. The data are available at https://legacy.openfmri.org/dataset/ds000243/.

2.1.2. Data acquisition

A Siemens MAGNETOM Tim TRIO 3.0T MRI scanner and a 12 channel Head Matrix Coil were used to obtain T1-weighted (MP-RAGE, 2.4s TR, 1x1x1mm voxels) and BOLD contrast sensitive (gradient echo EPI, 2.5s TR, 4x4x4mm voxels) images from each subject. The mean amount of BOLD data acquired per subject was 14 minutes (336 frames, range = 184-729 frames). Subjects were instructed to fixate on a black crosshair presented at the center of a white background. See Power et al., 2011 for full acquisition details.

2.1.3. Preprocessing

The first 12 frames (30 seconds) of each functional run were discarded to account for magnetization equilibrium and an auditory evoked response at the start of the EPI sequence (Laumann et al., 2015). Slice timing correction was applied first. Then, the functional data were aligned to the first frame of the first run using rigid body transforms, motion corrected (3D-cross realigned), and whole-brain mode 1000 normalized (Miezin et al., 2000). Next, the data were resampled (3 cubic mm voxels) and registered to the T1-weighted image and then to a WashU Talairach atlas (Ojemann et al., 1997) using affine transforms in a one-step operation (Smith et al., 2004).

Additional preprocessing of the resting-state BOLD data was applied to remove artifacts (Ciric et al., 2017; Power et al., 2014). Frame-wise displacement (FD) was calculated as

in Power et al., 2012, and frames with FD greater than 0.2 mm were censored. Uncensored segments with fewer than 5 contiguous frames were censored as well (mean +/- std frames retained = 279 +/- 107). All censored frames were interpolated over using least squares spectral estimation (Hocke and Kämpfer, 2009; Power et al., 2014). Next, the data were bandpass filtered from 0.009-0.08 Hz and nuisance regression was implemented. The regression included 36 regressors: the whole-brain mean, individually defined white matter and ventricular CSF signals, the temporal derivatives of each of these regressors, and an additional 24 movement regressors derived by expansion (Friston et al., 1996; Satterthwaite et al., 2012; Yan et al., 2013). FreeSurfer 5.3 automatic segmentation was applied to the T1-weighted images to create masks of the gray matter, white matter, and ventricles for the individual-specific regressors (Fischl et al., 2002). Finally, the data were smoothed with a Gaussian smoothing kernel (FWHM = 6 mm, sigma = 2.55).

At the end of all processing, each censored/interpolated frame was removed from the time series for all further analyses.

2.2. Secondary dataset- HCP 80

2.2.1. Dataset characteristics

Due to a partial cutoff of cerebellar data in the primary dataset (outside of the field of view), an independent secondary dataset was used to supplement analyses related to the cerebellum. This dataset was composed of 80 unrelated individuals from the Human Connectome Project (HCP) 500 Subject Release (40F, age range 22-35, mean age 28.4) with high quality (low-motion) data, described previously (Gordon et al., 2017a). All HCP data are available at https://db.humanconnectome.org.

2.2.2. Data acquisition

A custom Siemens SKYRA 3.0T MRI scanner and a custom 32 channel Head Matrix Coil were used to obtain high-resolution T1-weighted (MP-RAGE, 2.4s TR, 0.7x0.7x0.7mm voxels) and BOLD contrast sensitive (gradient echo EPI, multiband factor 8, 0.72s TR, 2x2x2mm voxels) images from each subject. The HCP used sequences with left-to-right and right-to-left phase encoding, with a single RL and LR run on each day for two consecutive days for a total of four runs (Van Essen et al., 2012). Thus, for symmetry, the BOLD time series from each subject's best (most frames retained after censoring) LR run and their best RL run were concatenated together.

2.2.3. Preprocessing

The preprocessing steps were the same as those detailed in Section 2.1.3 except for the following: (1) the first 41 frames (29.52 seconds) of each run were discarded, (2) no slice timing correction was applied, (3) field inhomogeneity distortion correction was applied (using the mean field map), (4) the data were not resampled (they were collected at 2 cubic mm isotropic voxels), and (5) the Gaussian smoothing kernel was

smaller (FWHM = 4 mm, sigma = 1.7). The first two changes are due to the increased temporal resolution of the HCP data acquisition (0.72s TR) and the last two changes are due to the increased spatial resolution of HCP data acquisition (Glasser et al., 2013). Distortion correction was not applied to the primary dataset because field maps were not collected in most participants. In addition, the increased temporal resolution caused respiration artifacts to alias into the FD trace (Fair et al., 2018; Siegel et al., 2017). Thus, FD values were filtered with a lowpass filter at 0.1 Hz and the filtered FD threshold was set at 0.1 mm (mean +/- std frames retained = 2236 +/- 76).

For the purpose of the winner-take-all partitioning of the secondary dataset (described in section 2.4), a CIFTI was created for each subject. Thus, preprocessed cortical BOLD time series data (from the secondary dataset only) were mapped to the surface, following the procedure of Gordon et al., 2016, and combined with volumetric subcortical and cerebellar data in the CIFTI format (Glasser et al., 2013; Gordon et al., 2016).

At the end of all processing, each censored/interpolated frame was removed from the time series for all further analyses.

2.3. Validation dataset- MSC

2.3.1. Dataset characteristics

Since the primary and secondary datasets were used to create the subcortical and cerebellar ROIs (described in sections 2.5 and 2.6), results for functional network community assignment (described in section 2.7) were validated with a third independent dataset, the Midnight Scan Club (MSC), described previously (Gordon et al., 2017b). These data are available at https://openneuro.org/datasets/ds000224/versions/00002. The MSC dataset consists of 5 hours of resting-state BOLD data from each of 10 individuals (5 F, age range 24-34, mean age 29) over a two-week period.

2.3.2. Data acquisition

The same scanner, head coil, and acquisition parameters described in Section 2.1.2 were used to for the MSC. However, a single resting-state run lasting 30 minutes was collected on 10 separate days. Each scan was acquired starting at midnight (Gordon et al., 2017b).

2.3.3. Preprocessing

For each subject, all runs were concatenated together in the order that they were collected. The initial preprocessing steps were the same as those detailed in Section 2.1.3 except for the following: (1) the functional images were registered to the average T2-weighted anatomical image (4 were collected per subject), then to the average T1-weighted anatomical image (4 were collected per subject), and finally to the Talairach

atlas, (2) field inhomogeneity distortion correction was applied (using the mean field map), and (3) one subject (MSC08) was excluded due to a substantial amount of low-quality data and self-reported sleeping during acquisition, as detailed previously (Gordon et al., 2017b; Laumann et al., 2016).

Additional preprocessing followed Marek and colleagues (Marek et al., 2018). Again, FD was used to exclude high-motion frames; however, due to respiratory artifacts affecting the realignment parameters (Power et al., 2018; Siegel et al., 2017), a lowpass filter (0.1 Hz) was applied to those parameters before calculation of FD. Consequently, the threshold for frame censoring was lowered to 0.1mm. Frames with outstanding (>2.5 standard deviations above the mode computed across all runs) DVARS values (as calculated in Power et al., 2012) were also excluded. All censored frames were interpolated over using least squares spectral estimation. After, a bandpass filter (0.005-0.1 Hz) was applied.

Finally, component-based nuisance regression was implemented. Individual-specific FreeSurfer 6.0 segmentation was used to define masks of the gray matter, white matter, and ventricles. A mask of extra-axial (or edge (Patriat et al., 2015)) voxels was also created by thresholding the temporal standard deviation image (>2.5%, excluding all voxels within a dilated whole-brain mask). BOLD data was extracted from all voxels in each mask (separately), and dimensionality reduction was applied as in CompCor (Behzadi et al., 2007). The number of components retained was determined independently for each mask such that the condition number (i.e., the maximum eigenvalue divided by the minimum eigenvalue) was greater than 30. All retained components were submitted to a regressors matrix that also included the 6 realignment parameters. To avoid collinearity, singular value decomposition was applied to the regressors covariance matrix. Components of this decomposition were retained up to an upper limit (condition number >=250). Then, all of the final retained components, the whole-brain mean, and its temporal derivative were regressed from the BOLD time series.

At the end of all processing, each censored/interpolated frame was removed from the time series for all further analyses.

2.4. Winner-take-all partitioning of the subcortex and cerebellum

In order to first identify functional subdivisions within subcortical structures and the cerebellum, a winner-take-all partitioning technique was applied to the basal ganglia, thalamus, and cerebellum, as previously described (Greene et al., 2014). Past applications of this winner-take-all approach have yielded results consistent with known connectivity from the animal literature (Buckner et al., 2011; Choi et al., 2012; Fair et al., 2010; Greene et al., 2014; Zhang et al., 2008).

Briefly, the mean resting-state time series were extracted from each of 11 previously defined cortical networks (Power et al., 2011): default mode, frontoparietal, cinguloopercular, salience, dorsal attention, ventral attention, visual, auditory,

somatomotor dorsal, somatomotor lateral, and orbitofrontal. In order to remove the shared variance among cortical networks thereby increasing specificity of the subcortico-cortical and cerebello-cortical correlations, partial correlations were then calculated between the time series from each cortical network and the resting-state time series from each subcortical or cerebellar gray matter voxel (e.g., for each cortical network and subcortical voxel, a residual correlation was computed after partialling out the signal from the other cortical networks). Each voxel was then assigned to the network with which it correlated most in a winner-take-all fashion (Buckner et al., 2011; Choi et al., 2012; Greene et al., 2014; Zhang et al., 2010), generating a functional partition of subcortical and cerebellar structures.

2.5. ROI creation

Spherical ROIs (diameter = 8mm) were placed in the (volumetric) center of each of the winner-take-all partitions in the basal ganglia, thalamus, and cerebellum. Then, the ROIs were manually adjusted such that (1) all ROIs included only gray matter voxels and (2) no ROIs had any overlapping voxels. Two additional ROIs (one per hemisphere) were added to the center of the amygdala based on anatomy (Talairach and Tournoux, 1988; Woolsey et al., 2008). Further, four ROIs (two per hemisphere) were added to the anterior and posterior portions of the hippocampus on the basis of the work from Kahn and colleagues (Kahn et al., 2008) that demonstrated distinct functional connectivity profiles for these two regions. In total, 34 subcortical and 27 cerebellar ROIs were created.

These new subcortical and cerebellar ROIs were then combined with two previously described sets of cortical ROIs from our lab, as follows:

ROI Set 1 (Power264 + new): Spherical cortical ROIs were used from the 264 volumetric ROIs reported in (Power et al., 2011). Four of these ROIs in the medial temporal lobe (two per hemisphere) were removed (Talairach coordinates: (-20, -24, -18), (17, -30, -15), (-25, -41, -8), (26, -39, -11)) and replaced by the four new hippocampus ROIs, due to some overlapping voxels. In addition, the 17 subcortical and cerebellar ROIs from the original 264 were replaced by 55 new subcortical and cerebellar ROIs. Finally, the 2 new amygdala ROIs were added. Thus, ROI Set 1 is composed of 239 cortical, 34 subcortical (including the amygdala and hippocampus), and 27 cerebellar volumetric ROIs, for a total of 300 ROIs.

ROI Set 2 (Gordon333 + new): ROI set 2 was generated by combining the 333 surface-based cortical parcels (Gordon et al., 2016) with the newly generated subcortical and cerebellar ROIs. Thus, ROI Set 2 is composed of 333 surface-based cortical parcels and 34 subcortical (including the amygdala and hippocampus) and 27 cerebellar volumetric ROIs, for a total of 394 ROIs. For all analyses using this ROI set, we utilized the center of each cortical parcel projected into volumetric atlas space (Gordon et al., 2016). The parcels in this format are publicly available at https://sites.wustl.edu/petersenschlaggarlab/parcels-19cwpgu/.

2.6. Seedmaps and consensus functional network communities for each ROI

2.6.1. Seedmaps

To validate the winner-take-all assignments of voxels used for ROI placement, we first conducted seedmap analyses to show how each ROI was correlated with every other gray matter voxel. A seedmap represents the pattern of correlations between the mean BOLD time series from a given ROI and all other gray matter voxels in the brain. We generated group-average seedmaps for both ROI Sets and each dataset (primary, secondary, validation). The preprocessed BOLD time series for each gray matter voxel within each ROI were averaged together (after removing censored and interpolated frames). Then, the Pearson correlation between each new ROI and every other gray matter voxel in the brain was computed for each subject. The subject-specific maps were Fisher transformed, averaged together, and inverse Fisher transformed.

2.6.2. Correlation matrices

We generated correlation matrices to examine the community structure of the new ROIs. A correlation matrix is the set of all possible pairwise correlations between mean BOLD time series from each ROI organized into a symmetric matrix (since correlations are undirected). We computed correlation matrices for both ROI Sets and each dataset (primary, secondary, validation). The preprocessed BOLD time series for each gray matter voxel within each ROI were averaged together (after removing censored and interpolated frames). Then, the Pearson correlation between every pair of ROIs was computed to create a 300 x 300 (ROI Set 1) and 394 x 394 (ROI set 2) correlation matrix for each subject. Each matrix was Fisher transformed, all matrices were averaged together (within each ROI set and dataset), and inverse Fisher transformed.

2.6.3. Community detection

To determine the functional network membership of each ROI, an information-theoretic community detection algorithm was implemented (InfoMap (Rosvall and Bergstrom, 2008)). InfoMap requires a sparse matrix, so an edge density threshold was applied to the correlation matrices. The networks (correlation matrices) were thresholded until only the strongest X percent of edges remained. We ran InfoMap over a range of thresholds (X = 2-10% inclusive, with a 1% step increment, following Power et al. (2011)).

In general, the magnitude of BOLD correlations between the cortex and the subcortex, the cortex and the cerebellum, and the subcortex and the cerebellum is substantially weaker than within-structure (and particularly, cortico-cortical) correlations. The primary reasons for this are distance from the head matrix coil and signal dropout due to sinuses. For instance, in the primary dataset, off-diagonal (between-structure) correlations from the subcortex and cerebellum account for 40% of the weakest decile of correlations (i.e., the 10% of correlations closest to 0), even though the subcortex and cerebellum account for only 23% of all ROIs. Therefore, in order to ensure that between-structure correlations were included, structure-specific thresholding was used

(Marek et al., 2018). The correlation matrix was separated into cortical, subcortical, and cerebellar components (e.g., the subcortical component is every entry in each row corresponding to any subcortical ROI) and the edge density thresholds were applied to each component separately. Thus, if a 2% structure-specific edge density was applied to the matrix, the top 2% of cortical, top 2% of subcortical, and top 2% of cerebellar correlations (excluding diagonal entries) were extracted and all other correlations were set to 0.

2.6.4. Consensus network procedure

Consensus functional network communities were determined in a semi-automated, multistep process. First, a weighting procedure was applied across InfoMap thresholds. For the 2% and 3% thresholds the weight was 5, for the 4% and 5% thresholds the weight was 3, and the weight was 1 for all other thresholds. These weights were chosen to bias the consensus solution to have approximately 17 networks on the basis of work from Yeo and colleagues (Yeo et al., 2011). Since smaller networks tend to show up at sparser thresholds, those thresholds contribute more weight than the denser thresholds. For each ROI (independently), the InfoMap-determined community at each threshold was noted, taking the weights into account, and the highest weighted community was assigned as the consensus.

After this automated consensus procedure, authors BAS, CG, and DJG reviewed the community assignment of each new subcortical and cerebellar ROI. In ambiguous cases (e.g., an even split in assignment across thresholds), we consulted literature describing the anatomy and function of that brain region. Consensus network communities were assigned in this way for 8 unclear cases (the 8 ROIs in the putamen).

All cortical ROIs retained their original assignment from published works (Power et al., 2011 for ROI Set 1 and from Gordon et al., 2016 for ROI Set 2) unless there was strong evidence to overturn the original. Specifically, if an ROI in the present InfoMap solution received the same assignment across all thresholds and that assignment was distinct from the original, then the ROI was assigned to the novel network community. Furthermore, 5 ROIs originally assigned to the salience network were reassigned to the cingulo-opercular network. We made this change because (1) the ROIs showed profiles intermediate between salience and cinguloopercular assignments and (2) previously published studies revealed that these brain regions demonstrate task-evoked activity consistent with the cingulo-opercular network (Dosenbach et al., 2006; Dubis et al., 2016; Gratton et al., 2018b, 2017; Neta et al., 2014).

2.6.5. Validation of consensus networks

The primary and secondary datasets were used to create the subcortical and cerebellar ROIs, respectively. The validation dataset (MSC) was used to test the validity of the consensus functional network communities in both cases. The network community assignment for each ROI was compared across all datasets, and discrepancies were

noted. Further, consensus networks were compared with those from previously published literature as well as anatomical atlases of brain regions.

2.7. Spring-embedded graphs

To visualize the community structure of networks in an abstract graph space, spring-embedded graphs were created. The networks (correlation matrices) were thresholded in the same way as in Section 2.6.3, and the resulting matrices were submitted to a physical model of connected springs (the Kamada-Kawai algorithm, as used in Power et al., 2011). Correlations between pairs of ROIs were modeled as force constants between connected springs such that strongly correlated ROIs were “pulled” close to one another. ROIs were colored according to their consensus functional network community or their anatomical location.

3. Results

3.1. Subcortical and cerebellar ROIs

The final set of subcortical and cerebellar ROIs overlaid onto the winner-take-all partitions are displayed in **Figure 1**. These winner-take-all partitions were similar to previously published partitions for the basal ganglia (Choi et al., 2012; Greene et al., 2014), thalamus (Hwang et al., 2017), and cerebellum (Buckner et al., 2011).

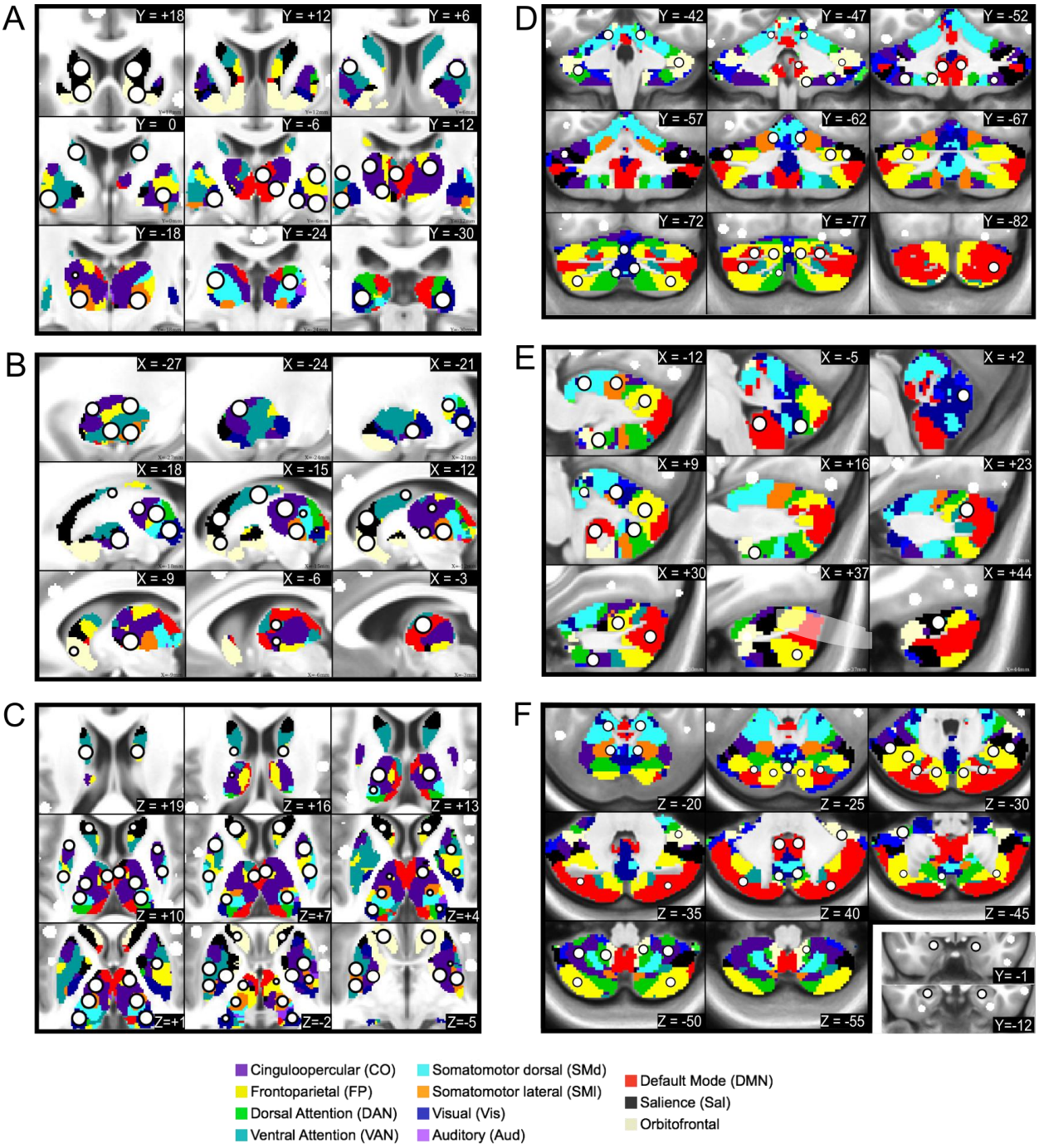

Figure 1: Subcortical and cerebellar ROIs. The new ROIs (white circle with black outline) are displayed in serial coronal (A and D), sagittal (B and E), and axial (C and F) sections for the subcortex in the left column (A, B, and C) and for the cerebellum in the right column (D, E, and F). The ROIs are overlaid on top of the voxel-wise winner-take-all partitioning, except for ROIs in the amygdala and anterior hippocampus, which are overlaid on anatomical coronal sections in the bottom right panel of F.

The 34 subcortical ROIs sampled the following anatomical structures (bilaterally): the head and tail of the caudate; anterior dorsal, posterior dorsal, anterior ventral, and posterior ventral putamen; the globus pallidus (internus and externus combined); the

ventral striatum (i.e., nucleus accumbens); the amygdala (nuclei not distinguished); anterior and posterior hippocampus; and regions in the thalamus. The locations of the thalamic ROIs included the following nuclei and surrounding territory (the resolution of our data was not fine enough to delineate precise thalamic nuclei): medio-dorsal (MD), latero-dorsal (LD), ventro-anterior (VA), ventro-lateral (VL), ventro-postero-lateral (VPL), and lateral geniculate nucleus (LGN)-pulvinar. The 27 cerebellar ROIs sampled the vestibulo-, spino-, and cerebro-cerebellum, including the cerebellar vermis, classical motor cerebellar cortex, and cerebellar association cortex (Woolsey et al., 2008).

3.2. Correlation structure replicates across datasets

Exemplar seedmaps for the primary dataset are displayed in **Figure 2** and the group-average correlation matrices for all datasets using ROI Set 1 are displayed in **Figure 3**. The correlation matrices using ROI Set 2 are displayed in SI Figure 1. The seedmaps were comparable to previously published maps (Figure 2). The matrices were quite similar across datasets ($r_{120,HCP} = 0.90$, $r_{120,MSC} = 0.93$, $r_{HCP,MSC} = 0.87$), with results from the primary dataset replicating best in the validation (MSC) dataset. However, in the secondary (HCP) dataset, there was approximately 0 correlation between subcortical ROIs and all other ROIs, including homotopic subcortical ROI pairs. The likely reason for this difference is due to poor temporal signal-to-noise ratio in the subcortex of HCP data (Ji et al., 2018), which we demonstrate here in SI Figure 2. Thus, we excluded the secondary dataset from all further analyses.

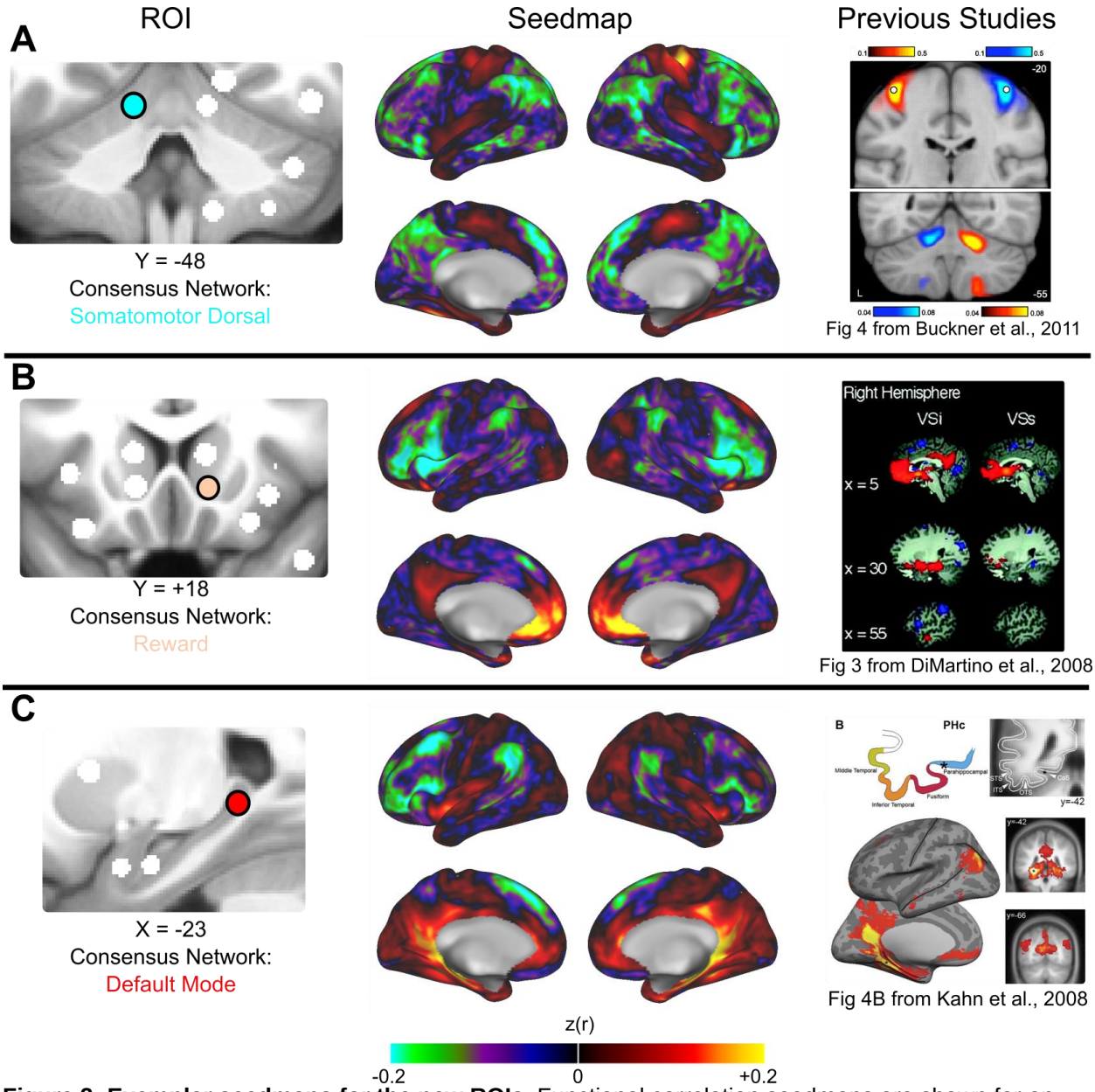

Figure 2: Exemplar seedmaps for the new ROIs. Functional correlation seedmaps are shown for an exemplar ROI in the cerebellum (A), basal ganglia (B), and hippocampus (C). The consensus functional network assignment of each ROI is represented by its color (left column). Seedmaps display the correlations between the mean BOLD signal from the ROI in question and the BOLD signal from every other gray matter voxel (middle column). Results were similar to comparable seedmaps from previously published studies (right column).

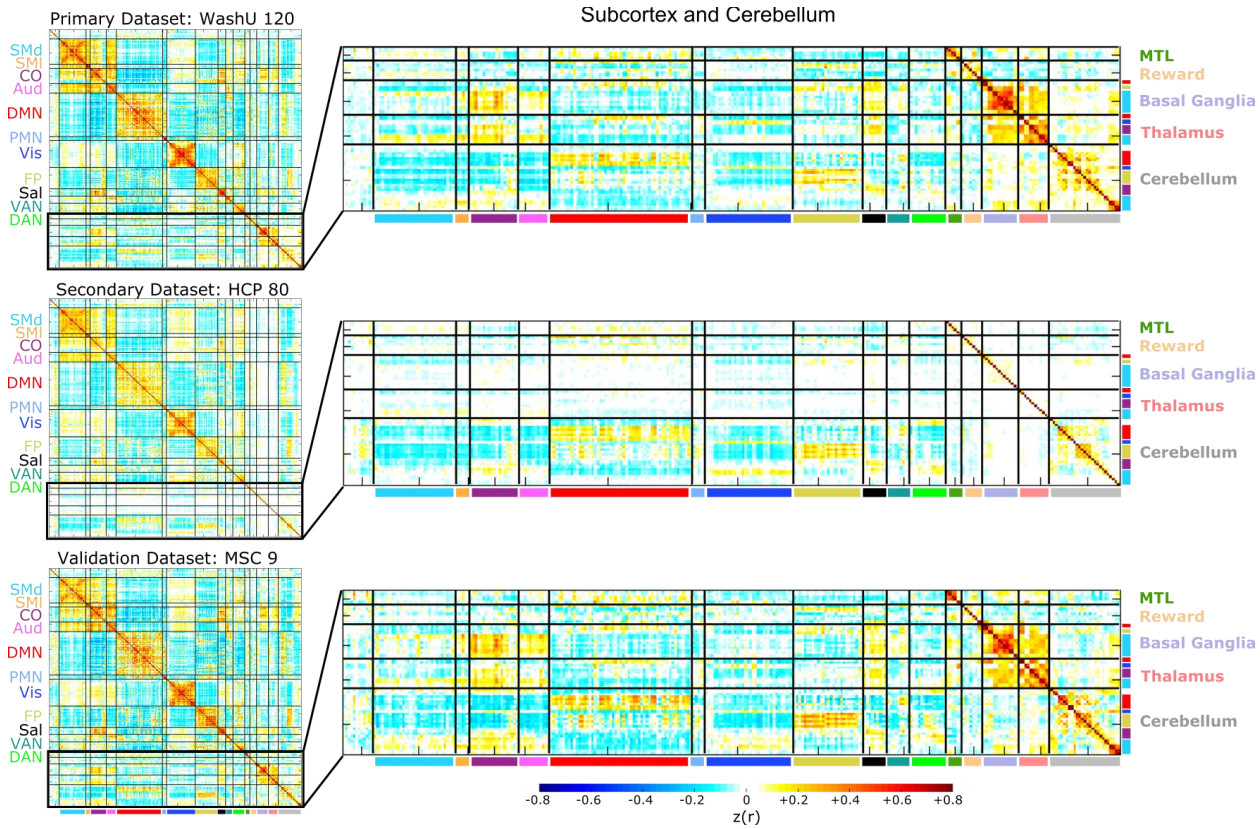

Figure 3: Correlation matrices are similar across datasets. The full (300 x 300) correlation matrices for ROI Set 1 are displayed for each dataset in the left column, and zoomed-in versions of the subcortical and cerebellar portions of the matrices are displayed in the right column (the corresponding images for ROI Set 2 are shown in SI Figure 1). The cortical portion of the correlation matrix is sorted by functional network community, whereas the subcortical and cerebellar portions are sorted first by anatomical structure (i.e., basal ganglia, thalamus, and cerebellum) and then by functional network community (within each structure). The matrices are quite similar (e.g., the correlation between the primary and validation datasets is 0.93), except for the subcortical portion of the secondary dataset (HCP- Human Connectome Project). We observed poor temporal signal-to-noise in subcortical HCP data (SI Figure 2).

3.3. Functional network organization using the expanded ROI Set

We used a data-driven community detection algorithm (InfoMap) to determine the functional network community membership of the expanded set of ROIs (Rosvall and Bergstrom, 2008). The results of this analysis are displayed in **Figure 4**. Communities are shown for all tested edge density thresholds alongside the consensus network communities (see section 2.6).

In the subcortex and cerebellum, the consensus network communities were as follows: ROIs in the caudate associated with the default mode network (head) or the frontoparietal network (tail). The putamen and globus pallidus ROIs joined the somatomotor dorsal network. In the thalamus, the default mode network was assigned to mediodorsal region, the cinguloopercular network to the laterodorsal and ventral anterior regions, the somatomotor dorsal network to the ventrolateral and ventral posteriolateral regions, and the visual network to the ROI that includes the lateral

geniculate nucleus and the posterior portion of the pulvinar. We use the names of the thalamic nuclei for convenience here, even though the ROIs encompass more gray matter than just the nuclei themselves. Cerebellar ROIs joined various networks, including the default mode, frontoparietal, and cinguloopercular networks (lateral), the somatomotor networks (motor cerebellar cortex), and the visual network (vermis). Most of the observed network assignments agree with known brain function, such as the association between ventral posteriolateral thalamic region and the somatomotor dorsal network.

While some ROIs did not vary in network membership across thresholds (e.g., the tail of the caudate ROIs), others changed network membership after a certain threshold (e.g., the putamen ROIs) or switched between two or more networks (e.g., some of the thalamic ROIs). This variation is similar to the variation seen with cortical ROI assignments (e.g., see Figure 1 from Power et al., 2011 and Figure 2A from Power et al., 2013) and is indicative of the loss of some finer-scale community structure at denser thresholds.

Importantly, we replicated these community assignments in the validation dataset (MSC; note that we did not use the secondary dataset for this analysis due to poor signal-to-noise in the subcortex). The consensus communities from the primary and validation datasets were broadly consistent across the two ROI Sets, with 55 out of 61 subcortical (including the amygdala and hippocampus) and cerebellar ROIs receiving the same assignment.

Most cortical ROIs retained their functional network membership from Power et al., 2011 (ROI Set 1) or Gordon et al., 2016 (ROI Set 2). Nonetheless, due to the addition of the new ROIs, we observed two functional networks not previously observed with the original ROI sets: (1) a network composed of ROIs in the amygdala, ventral striatum, orbitofrontal cortex, and ventral medial prefrontal cortex, which we will call the “reward” network and (2) a network composed of ROIs in the anterior hippocampus and entorhinal cortex, which we will call the “MTL” network. In addition, in ROI Set 1, 10 previously unlabeled ROIs were now assigned to a network: 4 to the reward network, 3 to the MTL network, 2 to the visual network, and 1 to the dorsal attention network. Also, 12 ROIs changed network membership: 2 from the cinguloopercular network to the somatomotor dorsal network, 1 from the auditory network to cinguloopercular network, and 9 from the salience network to the frontoparietal (2), dorsal attention (1), and cinguloopercular (6) networks. For ROI Set 2, 39 previously unlabeled ROIs were assigned to a network: 8 to the reward network, 10 to the MTL network, 16 to the parietooccipital network, and 5 to the default mode network (SI Figure 3). Again, consensus communities from the primary and validation datasets were broadly consistent.

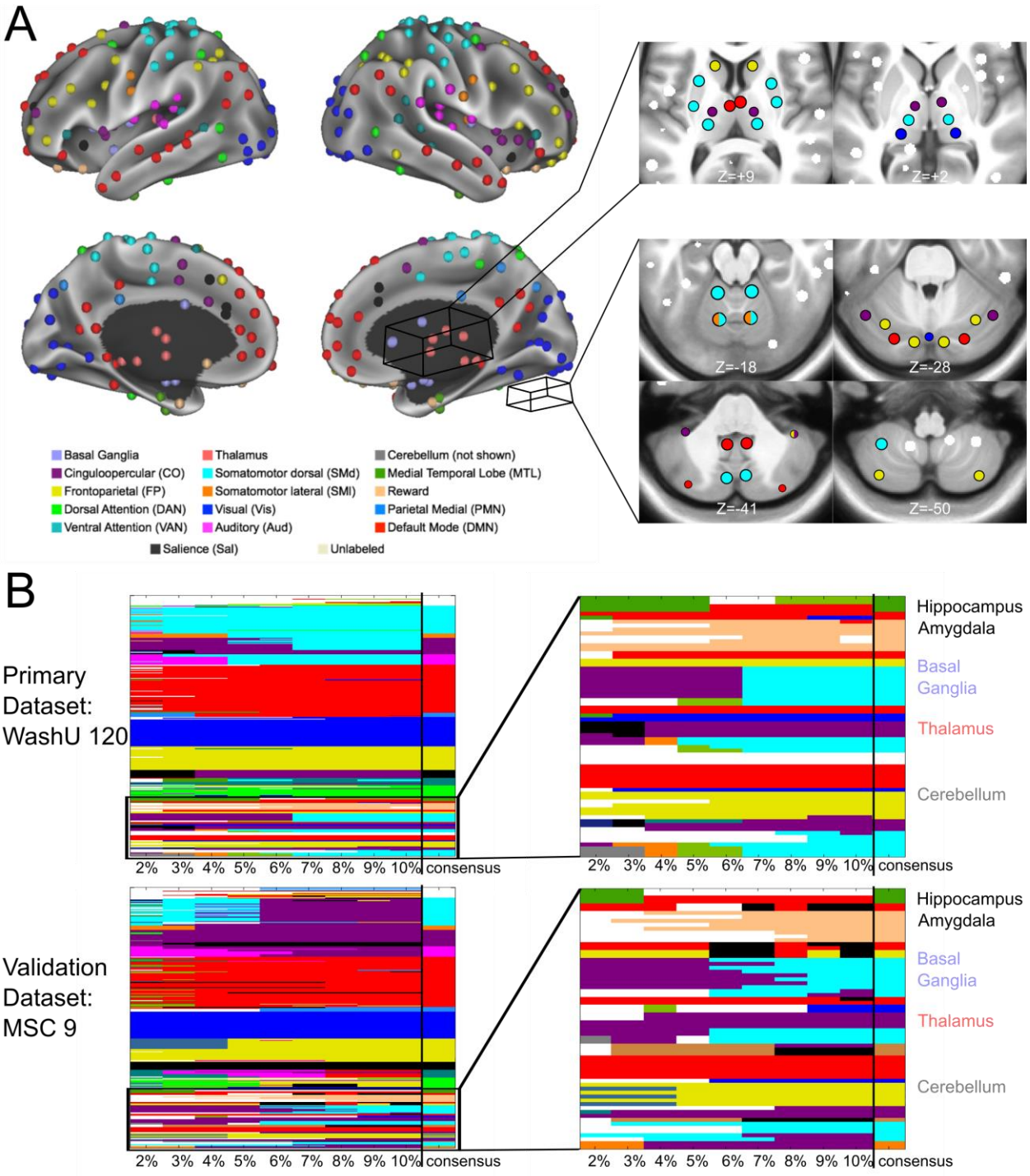

Figure 4: InfoMap-defined functional network communities. The InfoMap-defined functional network community of each ROI is displayed. (A) Cortical ROIs are shown projected onto the surface of the brain, and some of the non-cortical ROIs are displayed in axial slices to the right of the cortical surface. (B) The matrices represent the functional network assignment of each ROI across all tested edge densities, with the consensus functional network community displayed in the last column of each matrix (delineated by the vertical black line). Results are shown for the primary and validation datasets. The matrices on the right show zoomed-in results for all non-cortical ROIs. Results were highly consistent in the subcortex, cerebellum, amygdala, and hippocampus, with a total of 3 disagreements between datasets (in addition to 3 unlabeled ROIs at the bottom of the cerebellum forming their own “network” in the MSC dataset).

3.4. Subcortical and cerebellar ROIs integrate with known functional networks

To visualize the ROIs in functional network space, we created spring-embedded graphs, displayed in **Figure 5** (other edge densities in SI Figure 4). The implemented spring model aggregates nodes with strong correlations between themselves and weak correlations with other nodes. Thus, it is possible to observe which nodes segregate into separate communities and which nodes act as connector hubs, mediating interactions across different network communities (Gordon et al., 2018).

As is evident from the position of the bolded network nodes, the subcortical and cerebellar ROIs were distributed throughout the spring-embedded graph. For instance, the cerebellar ROIs (gray) were not segregated from the rest of the network communities as in previous reports (Gratton et al., 2018a; Power et al., 2011). This finding was consistent between the primary and validation datasets. However, we observed that the basal ganglia, thalamus, and cerebellum did segregate into their own network communities when the graph was created without structure-specific edge density thresholding (SI Figure 4; see Section 2.6.3 for the thresholding procedure). That is, the basal ganglia, thalamus, and cerebellum clustered into their own separate network communities with standard edge density thresholding (applying the threshold uniformly to the whole correlation matrix), likely because of the lower correlation magnitudes associated with these regions.

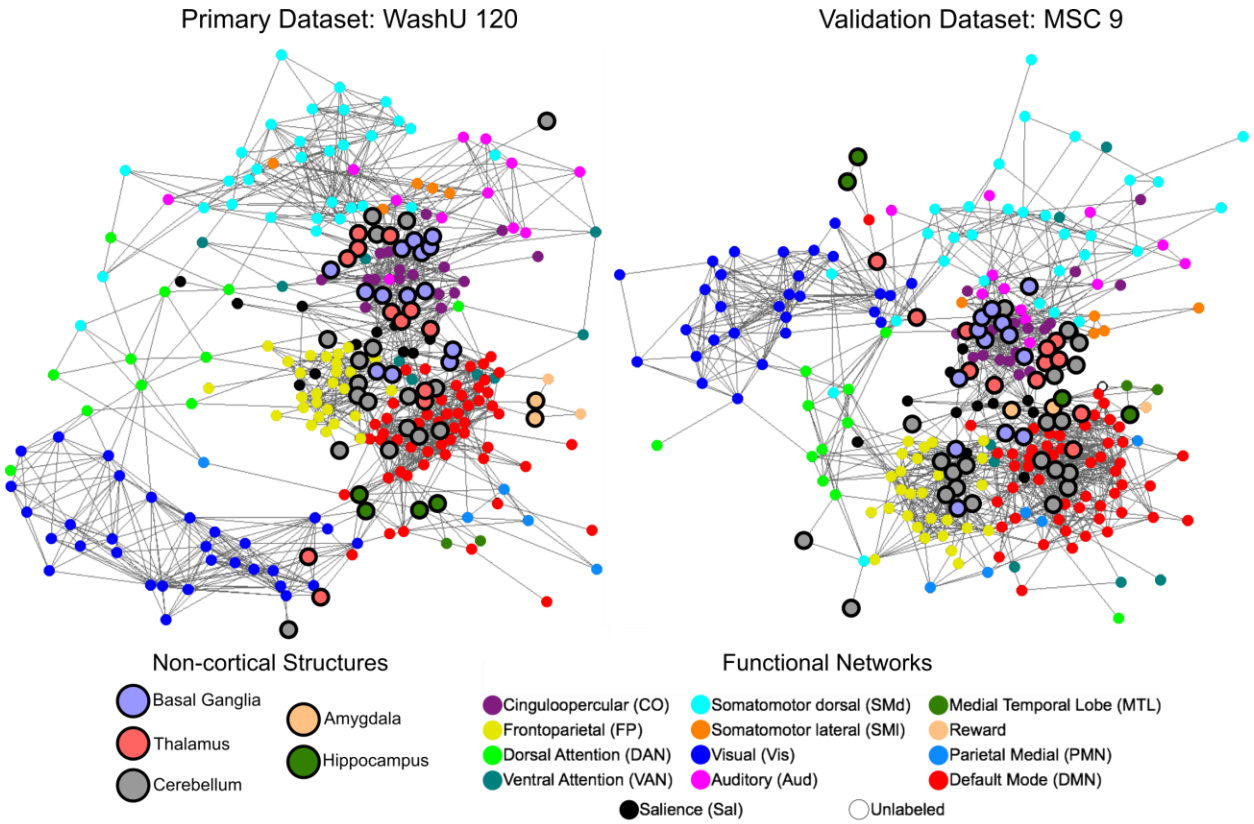

Figure 5- Spring-embedded graphs show that subcortical and cerebellar ROIs integrate with well-characterized network communities. Spring-embedded graphs are displayed for ROI Set 1 using the primary and validation datasets at a structure-specific edge density threshold of 3% (other edge densities shown in SI Figure 4; see section 2.6.3 for the thresholding procedure). Non-cortical ROIs are larger and have a bold outline. The color of each ROI represents its consensus functional network community assignment, except for the non-cortical ROIs, which are labeled by anatomical structure. The basal ganglia, thalamus, and cerebellum distribute throughout the graph, integrating with well-characterized networks rather than segregating into their own communities.

4. Discussion

Here we present a set of regions of interest (ROIs) that sample the basal ganglia, thalamus, cerebellum, amygdala, and hippocampus more completely than previous ROI sets in order to provide a whole-brain description of functional network organization. We found that the refined region sets recapitulate previous network organization results in the cortex and extend functional brain network characterization to the subcortex and cerebellum. Notably, these results replicated across independent datasets. In addition, due to the inclusion of the new ROIs, we observe two additional functional networks that were not present in Power et al. (2011) and Gordon et al. (2016): a reward network and a medial temporal lobe (MTL) network.

4.1. Improved sampling of the subcortex and cerebellum

Many recent research efforts have used the 264 ROIs from Power et al., 2011 or the 333 surface-based parcels from Gordon et al., 2016 to study brain network organization.

These studies have examined both structural and functional network organization in a wide variety of samples, including healthy young adults (Power et al., 2013; Zanto and Gazzaley, 2013), developmental cohorts (Gu et al., 2015; Nielsen et al., 2018; Rudolph et al., 2017), older adults (Baniqued et al., 2018; Gallen et al., 2016), and a plethora of neurological and psychiatric populations (Gratton et al., 2018a; Greene et al., 2016; Sheffield et al., 2015; Siegel et al., 2018). We have gained a better understanding of typical and atypical human brain organization from these efforts. However, a full characterization of whole-brain network organization in these populations is incomplete due to the underrepresentation of the subcortex and cerebellum.

The functionally-defined subcortical and cerebellar ROIs presented in the current work provide a better sampling of these structures. By improving the representation of these important brain structures, we were able to delineate well-characterized and additional functional network communities (relative to our past descriptions). The ability to uncover these networks, which have been previously described using other methods, illustrates the importance of representing the entire brain in network-based analyses. Further, these improved ROI sets may allow future studies to discover previously unobserved, yet critical deviations in functional network organization in diseases and disorders in which the subcortex and cerebellum are implicated (e.g., Parkinson Disease, Tourette Syndrome, Schizophrenia).

It is worth noting that, by definition, the cortical surface parcels omit the subcortex and cerebellum. Yet, it is technically possible to parcellate the subcortex and cerebellum using an adapted gradient-based methodology (such as the one from Gordon et al., 2016). This approach would require extending the gradient technique to 3 dimensions. As fMRI technology and analysis strategies improve, it would be useful to compare the current results to a full subcortical and cerebellar parcellation using this or other gradient-based techniques.

4.2. Functional connectivity of the refined ROIs is consistent with previous studies and replicates across independent datasets

Correlation seedmaps from the refined ROIs agree with functional connectivity profiles reported in previous studies. For example, the ROIs added to the ventral striatum and the head of the caudate correspond closely to the seeds placed in the superior ventral striatum (VSs) and dorsal caudate (DC) reported in Di Martino et al., 2008, and our seedmaps are highly similar to theirs. Likewise, seedmaps from the hippocampus and amygdala agree well with those from Kahn et al., 2008 and Roy et al., 2009, respectively. The same is true for the thalamus (Hwang et al., 2017) and cerebellum (Buckner et al., 2011).

Moreover, the full correlation structure (shown in correlation matrices) was quite comparable across the diverse datasets. The one major discrepancy was that in the subcortical portion of the matrix from the secondary (HCP) dataset we observed correlations near zero. The reason for this observation is likely poor temporal signal-to-noise ratio (tSNR) in the subcortex of HCP data (Ji et al., 2018). Several factors may

contribute to this poor tSNR: (1) The HCP used a custom scanner and coil, which caused unique magnetic field inhomogeneities, possibly in part due to subjects' heads being outside of the isocenter of the field. (2) The imaging sequence used an aggressive multiband factor and TR (MB = 8, TR = 0.72s) and (3) small voxels (2 cubic mm) were used for acquisition (Glasser et al., 2013; Van Essen et al., 2012). Each of these factors substantially increase electronic, thermal, and other physical sources of noise (Triantafyllou et al., 2005) relative to slower sequences with larger voxels. These effects may be amplified as a function of the distance of the imaged structure from the head coil, resulting in the poorest tSNR in the subcortex. Further work is needed to determine the specific contributions of each factor, as well as others heretofore unconsidered, to the observed poor tSNR.

The presented group-level descriptions converge on a very similar picture of functional network organization in the subcortex and cerebellum. However, it is likely that there are individual differences in both subcortical and cerebellar functional network organization, as have been found in cortical functional network organization. Future work designed for in-depth study of individuals, as in Poldrack et al., (2015), Braga and Buckner (2017), and Gordon et al. (2017b), will be important for elucidating such individual differences. In fact, in-depth study of the cerebellum in individuals reveals both common and unique features in its functional organization (Marek et al., 2018).

4.3. Reward and MTL functional networks map onto known human brain systems

Group-average functional network organization in the cerebral cortex is largely consistent across studies (Power et al., 2011; Yeo et al., 2011), and the addition of refined subcortical and cerebellar ROIs did not change functional network organization in the cortex substantially (although we observed associations between these canonical networks and ROIs in the subcortex and cerebellum). However, the addition of these subcortical and cerebellar ROIs allowed for the identification of two additional functional networks compared to the original ROI sets reported in Power et al. (2011) and Gordon et al. (2016): (1) a "reward" network composed of the amygdala, orbitofrontal cortex, and ventromedial prefrontal cortex, and (2) a "medial temporal lobe (MTL)" network composed of the anterior hippocampus and entorhinal cortex. It is worth noting that the reward network has been observed in studies focusing on reward processing (Camara et al., 2009) and its cortical portion is very similar to the limbic network from Yeo et al., (2011). The MTL network has been observed in a study of highly-sampled individuals (Gordon et al., 2017b) as well as studies focused on the hippocampus (Greicius et al., 2009). Here, we demonstrate that these networks are measurable at the group-level when the whole brain is represented sufficiently. In addition, we found that some cortical ROIs that were previously unlabeled (i.e., they did not group with any community) received labels with the inclusion of the refined subcortical and cerebellar ROIs, with many of them joining the reward and MTL networks.

The reward and MTL functional networks map onto well-characterized brain systems. Most of the ROIs in the reward network are connected to each other anatomically in rodents, nonhuman primates, and humans (Ongur and Price, 2000; Carmichael and

Price, 1995; Amaral and Price, 1984). Moreover, these brain areas are known to be functionally related, as they are important for various aspects of decision making and reward-related behavior, such as economic choice (Padoa-Schioppa and Assad, 2006), emotional regulation (Phelps, 2006), and gambling (Bechara et al., 2000, 1997). Likewise, the ROIs in the MTL network are well-connected anatomically (Duvernoy, 1988; Woolsey et al., 2008) and support various aspects of memory formation, consolidation, and retrieval, as well as other important functions, such as spatial mapping (Burgess et al., 2002; Moser and Moser, 1998; Tulving and Markowitsch, 1998). Though our current work is agnostic to the function of these brain systems, we show that their constituent regions demonstrate coherent spontaneous fluctuations in the BOLD signal.

4.4. Subcortical and cerebellar ROIs integrate with known functional networks

To visualize the organization of the ROIs in functional network space, we created spring-embedded graphs. We observed that the subcortical and cerebellar ROIs integrate with various well-characterized network communities composed of cortical regions instead of segregating on their own (i.e., away from cortical ROIs). This organization fits with the known anatomy and function of the subcortex and cerebellum better than a model in which each structure is segregated into its own community. For instance, individual nuclei in the thalamus project directly to distinct brain systems (Woolsey et al., 2008) and play unique roles in behaviors associated with those systems (Guillery, 1995; Van Der Werf et al., 2000). Likewise, striato-cortical and cerebello-cortical anatomical connections show specific projections to unique regions of cortex (Woolsey et al., 2008) and are known to be integral for the function of various large-scale, distributed systems, such as the motor system (Glickstein and Doron, 2008) and regions of higher order systems (Alexander et al., 1986; Strick et al., 2009).

This finding of integration was revealed by the use of structure-specific edge density thresholding (i.e., thresholding the cortex, subcortex, and cerebellum separately). In most network analyses, only the strongest positive correlations are considered for network-based analyses, such as spring-embedded graphs. However, subcortical correlations are generally weaker than cortical correlations. Thus, if the top 5% strongest positive correlations are selected, almost all subcortical correlations will be excluded. To avoid this exclusion, we implemented structure-specific thresholding. This choice ultimately affects the nature of the spring-embedded graph as well as the determination of functional network communities. Without structure-specific thresholding, subcortical ROIs group with one another into two separate network communities (basal ganglia and thalamus), while the entire cerebellum is lumped into one network community. In terms of human brain functional organization, this pattern of anatomical clustering seems artificially inflated due to low subcortex-to-cortex and cerebellum-to-cortex correlations. By using structure-specific thresholding, we were able to observe functional network organization that is more consistent with the known functions of the subcortex and cerebellum.

There are advantages to both anatomical and functional network-based divisions of ROIs. For instance, anatomical network divisions allow for analysis of important distinctions between the cortex, subcortex, and cerebellum, whereas functional network divisions better represent putative brain function. Ultimately, researchers should be cognizant of these effects when choosing how to perform network-based analyses.

4.5. Conclusions

We created new subcortical and cerebellar ROIs to improve the representation of these important structures for brain network analysis. Combining these new ROIs with previously characterized cortical ROIs allowed further insight into whole-brain functional network organization. Going forward, inclusion of these ROIs will yield more comprehensive results from fMRI studies of typical and atypical brain organization and function. The ROI Sets and consensus functional network assignments described here are available for immediate download and use at https://greenelab.wustl.edu/data_software.

Acknowledgements

This work was supported by National Institutes of Health grants T32 NS073547 (BAS), F32 NS092290 (CG), T32 MH10001902 (SM), K23 NS088590 (NUFD), UL1 TR000448 (NUFD), R01 NS32979 (SEP), R01 NS06424 (SEP), and K01 MH104592 (DJG); the Jacobs Foundation grant 2016121703 (NUFD); the Child Neurology Foundation (NUFD); the Mallinckrodt Institute of Radiology grant 14-011 (NUFD); the Hope Center for Neurological Disorders (NUFD, BLS, SEP); a McDonnell Foundation Collaborative Activity Award (SEP); the McDonnell Center for Systems Neuroscience (NUFD, BLS, DJG); and, the Tourette Association of America (DJG).

Author Contributions

BAS, CG, and DJG designed the study. BAS, CG, SM, RVR, and DJG analyzed the data. All authors wrote the manuscript.

Competing Interests

All authors declare no competing interests.

References

Alexander, G.E., DeLong, M.R., Strick, P.L., 1986. Parallel Organization of Functionally Segregated Circuits Linking Basal Ganglia and Cortex. Annu. Rev. Neurosci. 9, 357–381. doi:10.1146/annurev.neuro.9.1.357

Allman, J.M., Kaas, J.H., 1971. A representation of the visual field in the caudal third of the middle tempral gyrus of the owl monkey (Aotus trivirgatus). Brain Res. 31, 85–105. doi:10.1016/0006-8993(71)90635-4

Andreasen, N.C., Nopoulos, P., O'Leary, D.S., Miller, D.D., Wassink, T., Flaum, M., 1999. Defining the phenotype of schizophrenia: Cognitive dysmetria and its neural mechanisms. Biol. Psychiatry. doi:10.1016/S0006-3223(99)00152-3

Andreasen, N.C., O'Leary, D.S., Cizadlo, T., Arndt, S., Rezai, K., Ponto, L.L., Watkins, G.L., Hichwa, R.D., 1996. Schizophrenia and cognitive dysmetria: a positron-emission tomography study of dysfunctional prefrontal-thalamic-cerebellar circuitry. Pnas 93, 9985–9990. doi:10.1073/pnas.93.18.9985

Baniqued, P.L., Gallen, C.L., Voss, M.W., Burzynska, A.Z., Wong, C.N., Cooke, G.E., Duffy, K., Fanning, J., Ehlers, D.K., Salerno, E.A., Aguiñaga, S., McAuley, E., Kramer, A.F., D'Esposito, M., 2018. Brain network modularity predicts exercise-related executive function gains in older adults. Front. Aging Neurosci. 9. doi:10.3389/fnagi.2017.00426

Bassett, D.S., Bullmore, E., 2006. Small-world brain networks. Neuroscientist 12, 512–523. doi:10.1177/1073858406293182

Bechara, A., Damasio, H., Damasio, A.R., 2000. Emotion,Decision Making and the Orbitofrontal Cortex. Cereb. Cortex 10, 295–307. doi:10.1093/cercor/10.3.295

Bechara, A., Damasio, H., Tranel, D., Damasio, A.R., 1997. Deciding advantageously before knowing the advantageous strategy. Science (80-.). 275, 1293–1295. doi:10.1126/science.275.5304.1293

Behzadi, Y., Restom, K., Liau, J., Liu, T.T., 2007. A component based noise correction method (CompCor) for BOLD and perfusion based fMRI. Neuroimage 37, 90–101. doi:10.1016/j.neuroimage.2007.04.042

Bigelow, N.O., Turner, B.M., Andreasen, N.C., Paulsen, J.S., O'Leary, D.S., Ho, B.C., 2006. Prism adaptation in schizophrenia. Brain Cogn. 61, 235–242. doi:10.1016/j.bandc.2006.01.004

Biswal, B., Yetkin, F.Z., Haughton, V.M., Hyde, J.S., 1995. Functional connectivity in the motor cortex of resting human brain using echo-planar MRI. Magn. Reson. Med. 34, 537–541. doi:10.1002/mrm.1910340409

Bondy, J.A., Murty, U.S.R., 1976. Graph theory with applications. Graph Theory. doi:10.2307/3008805

Bostan, A.C., Strick, P.L., 2018. The basal ganglia and the cerebellum: nodes in an integrated network. Nat. Rev. Neurosci. 1–13. doi:10.1038/s41583-018-0002-7

Braga, R.M., Buckner, R.L., 2017. Parallel Interdigitated Distributed Networks within the Individual Estimated by Intrinsic Functional Connectivity. Neuron 95, 457–471.e5. doi:10.1016/j.neuron.2017.06.038

Brown, S.M., Kieffaber, P.D., Carroll, C.A., Vohs, J.L., Tracy, J.A., Shekhar, A., O'Donnell, B.F., Steinmetz, J.E., Hetrick, W.P., 2005. Eyeblink conditioning deficits indicate timing and cerebellar abnormalities in schizophrenia. Brain Cogn. 58, 94–108. doi:10.1016/j.bandc.2004.09.011

Buckner, R.L., Krienen, F.M., Castellanos, a., Diaz, J.C., Yeo, B.T.T., 2011. The organization of the human cerebellum estimated by intrinsic functional connectivity. J. Neurophysiol. 106, 2322–2345. doi:10.1152/jn.00339.2011

Bullmore, E., Sporns, O., 2009. Complex brain networks: graph theoretical analysis of structural and functional systems. Nat. Rev. Neurosci. 10, 186–98. doi:10.1038/nrn2575

Bullmore, E.T., Bassett, D.S., 2011. Brain Graphs: Graphical Models of the Human Brain Connectome. Annu. Rev. Clin. Psychol. 7, 113–140. doi:10.1146/annurev-clinpsy-040510-143934

Burgess, N., Maguire, E. a, O'Keefe, J., 2002. The human hippocampus and spatial and episodic memory 1. Neuron 35, 625–641. doi:10.1016/S0896-6273(02)00830-9

Butts, C.T., 2009. Revisiting the foundations of network analysis. Science (80-.). doi:10.1126/science.1171022

Butts, C.T., 2008. Social network analysis: A methodological introduction. Asian J. Soc. Psychol. 11, 13–41. doi:10.1111/j.1467-839X.2007.00241.x

Camara, E., Rodriguez-Fornells, A., Münte, T.F., 2009. Functional connectivity of reward processing in the brain. Front. Hum. Neurosci. 2, 19. doi:10.3389/neuro.09.019.2008

Choi, E.Y., Yeo, B.T.T., Buckner, R.L., 2012. The organization of the human striatum estimated by intrinsic functional connectivity. J. Neurophysiol. 108, 2242–63. doi:10.1152/jn.00270.2012

Ciric, R., Wolf, D.H., Power, J.D., Roalf, D.R., Baum, G., Ruparel, K., Shinohara, R.T., Elliott, M.A., Eickhoff, S.B., Davatzikos, C., Gur, R.C., Gur, R.E., Bassett, D.S.,

Satterthwaite, T.D., 2017. Benchmarking confound regression strategies for the control of motion artifact in studies of functional connectivity. Neuroimage 154, 174–187. doi:10.1016/j.neuroimage.2017.03.020

Cohen, A.L., Fair, D.A., Dosenbach, N.U.F., Miezin, F.M., Dierker, D., Van Essen, D.C., Schlaggar, B.L., Petersen, S.E., 2008. Defining functional areas in individual human brains using resting functional connectivity MRI. Neuroimage 41, 45–57. doi:10.1016/j.neuroimage.2008.01.066

Corbetta, M., Shulman, G.L., 2011. Spatial neglect and attention networks. Annu. Rev. Neurosci. 34, 569–99. doi:10.1146/annurev-neuro-061010-113731

Craddock, R.C., James, G.A., Holtzheimer, P.E., Hu, X.P., Mayberg, H.S., 2012. A whole brain fMRI atlas generated via spatially constrained spectral clustering. Hum. Brain Mapp. 33, 1914–1928. doi:10.1002/hbm.21333

Di Martino, A., Scheres, A., Margulies, D.S., Kelly, A.M.C., Uddin, L.Q., Shehzad, Z., Biswal, B., Walters, J.R., Castellanos, F.X., Milham, M.P., 2008. Functional Connectivity of Human Striatum: A Resting State fMRI Study. Cereb. Cortex 18, 2735–2747. doi:10.1093/cercor/bhn041

Dosenbach, N.U.F., Visscher, K.M., Palmer, E.D., Miezin, F.M., Wenger, K.K., Kang, H.C., Burgund, E.D., Grimes, A.L., Schlaggar, B.L., Petersen, S.E., 2006. A Core System for the Implementation of Task Sets. Neuron 50, 799–812. doi:10.1016/j.neuron.2006.04.031

Dubis, J.W., Siegel, J.S., Neta, M., Visscher, K.M., Petersen, S.E., 2016. Tasks Driven by Perceptual Information Do Not Recruit Sustained BOLD Activity in Cingulo-Opercular Regions. Cereb. Cortex 26, 192–201. doi:10.1093/cercor/bhu187

Duvernoy, H.M., 1988. The Human Hippocampus: An Atlas of Applied Anatomy, JF Bergmann Munich. doi:10.1007/978-3-642-54195-7

Fair, D.A., Bathula, D., Mills, K.L., Costa Dias, T.G., Blythe, M.S., Zhang, D., Snyder, A.Z., Raichle, M.E., Stevens, A.E., Nigg, J.T., Nagel, B.J., 2010. Maturing thalamocortical functional connectivity across development. Front. Syst. Neurosci. doi:10.3389/fnsys.2010.00010

Fair, D.A., Miranda-Dominguez, O., Snyder, A.Z., Perrone, A.A., Earl, E.A., Van, A.N., Koller, J.M., Feczko, E., Klein, R.L., Mirro, A.E., Hampton, J.M., Adeyemo, B., Laumann, T.O., Gratton, C., Greene, D.J., Schlaggar, B., Hagler, D., Watts, R., Garavan, H., Barch, D.M., Nigg, J.T., Petersen, S.E., Dale, A., Feldstein-Ewing, S.W., Nagel, B.J., Dosenbach, N.U.F., 2018. Correction of respiratory artifacts in MRI head motion estimates. bioRxiv.

Fatemi, S.H., Halt, A.R., Realmuto, G., Earle, J., Kist, D.A., Thuras, P., Metz, A., 2002. Purkinje cell size is reduced in cerebellum of patients with autism. Cell. Mol. Neurobiol. 22, 171–175. doi:10.1023/A:1019861721160

Felleman, D.J., Van Essen, D.C., 1991. Distributed hierarchical processing in the primate cerebral cortex. Cereb. Cortex 1, 1–47. doi:10.1093/cercor/1.1.1

Fiez, J.A., 2016. The cerebellum and language: Persistent themes and findings. Brain Lang. 161, 1–3. doi:10.1016/j.bandl.2016.09.004

Fischl, B., Salat, D.H., Busa, E., Albert, M., Dieterich, M., Haselgrove, C., Van Der Kouwe, A., Killiany, R., Kennedy, D., Klaveness, S., Montillo, A., Makris, N., Rosen, B., Dale, A.M., 2002. Whole brain segmentation: Automated labeling of neuroanatomical structures in the human brain. Neuron 33, 341–355. doi:10.1016/S0896-6273(02)00569-X

Friston, K.J., Williams, S., Howard, R., Frackowiak, R.S.J., Turner, R., 1996. Movement-related effects in fMRI time-series. Magn. Reson. Med. 35, 346–355. doi:10.1002/mrm.1910350312

Gallen, C.L., Baniqued, P.L., Chapman, S.B., Aslan, S., Keebler, M., Didehbani, N., D'Esposito, M., 2016. Modular brain network organization predicts response to cognitive training in older adults. PLoS One 11. doi:10.1371/journal.pone.0169015

Glasser, M.F., Coalson, T.S., Robinson, E.C., Hacker, C.D., Harwell, J., Yacoub, E., Ugurbil, K., Andersson, J., Beckmann, C.F., Jenkinson, M., Smith, S.M., Van Essen, D.C., 2016. A multi-modal parcellation of human cerebral cortex. Nature 536, 171–8. doi:10.1038/nature18933

Glasser, M.F., Sotiropoulos, S.N., Wilson, J.A., Coalson, T.S., Fischl, B., Andersson, J.L., Xu, J., Jbabdi, S., Webster, M., Polimeni, J.R., Van Essen, D.C., Jenkinson, M., 2013. The minimal preprocessing pipelines for the Human Connectome Project. Neuroimage 80, 105–124. doi:10.1016/j.neuroimage.2013.04.127

Glickstein, M., Doron, K., 2008. Cerebellum: Connections and Functions. Cerebellum 7, 589–594. doi:10.1007/s12311-008-0074-4

Gordon, E.M., Laumann, T.O., Adeyemo, B., Gilmore, A.W., Nelson, S.M., Dosenbach, N.U.F., Petersen, S.E., 2017a. Individual-specific features of brain systems identified with resting state functional correlations. Neuroimage 146, 918–939. doi:10.1016/j.neuroimage.2016.08.032

Gordon, E.M., Laumann, T.O., Adeyemo, B., Huckins, J.F., Kelley, W.M., Petersen, S.E., 2016. Generation and Evaluation of a Cortical Area Parcellation from Resting-State Correlations. Cereb. Cortex 26, 288–303. doi:10.1093/cercor/bhu239

Gordon, E.M., Laumann, T.O., Gilmore, A.W., Newbold, D.J., Greene, D.J., Berg, J.J., Ortega, M., Hoyt-Drazen, C., Gratton, C., Sun, H., Hampton, J.M., Coalson, R.S., Nguyen, A.L., McDermott, K.B., Shimony, J.S., Snyder, A.Z., Schlaggar, B.L., Petersen, S.E., Nelson, S.M., Dosenbach, N.U.F., 2017b. Precision Functional Mapping of Individual Human Brains. Neuron 95, 791–807.e7. doi:10.1016/j.neuron.2017.07.011

Gordon, E.M., Lynch, C.J., Gratton, C., Laumann, T.O., Gilmore, A.W., Greene, D.J., Ortega, M., Nguyen, A.L., Schlaggar, B.L., Petersen, S.E., Dosenbach, N.U.F., Nelson, S.M., 2018. Three Distinct Sets of Connector Hubs Integrate Human Brain Function. Cell Rep. 24, 1687–1695.e4. doi:10.1016/j.celrep.2018.07.050

Gratton, C., Koller, J.M., Shannon, W., Greene, D.J., Snyder, A.Z., Petersen, S.E., Perlmutter, J.S., Campbell, M.C., 2018a. Emergent Functional Network Effects in Parkinson Disease. Cereb. Cortex 1–15. doi:10.1093/cercor/bhy121

Gratton, C., Neta, M., Sun, H., Ploran, E.J., Schlaggar, B.L., Wheeler, M.E., Petersen, S.E., Nelson, S.M., 2017. Distinct Stages of Moment-to-Moment Processing in the Cinguloopercular and Frontoparietal Networks. Cereb. Cortex 27, 2403–2417. doi:10.1093/cercor/bhw092

Gratton, C., Sun, H., Petersen, S.E., 2018b. Control networks and hubs. Psychophysiology. doi:10.1111/psyp.13032

Greene, D.J., Black, K.J., Schlaggar, B.L., 2013. Neurobiology and functional anatomy of tic disorders. Tourette Syndr. doi:http://dx.doi.org/10.1093/med/9780199796267.003.0012

Greene, D.J., Church, J.A., Dosenbach, N.U.F., Nielsen, A.N., Adeyemo, B., Nardos, B., Petersen, S.E., Black, K.J., Schlaggar, B.L., 2016. Multivariate pattern classification of pediatric Tourette syndrome using functional connectivity MRI. Dev. Sci. 19, 581–598. doi:10.1111/desc.12407

Greene, D.J., Laumann, T.O., Dubis, J.W., Ihnen, S.K., Neta, M., Power, J.D., Pruett, J.R., Black, K.J., Schlaggar, B.L., 2014. Developmental changes in the organization of functional connections between the basal ganglia and cerebral cortex. J. Neurosci. 34, 5842–54. doi:10.1523/JNEUROSCI.3069-13.2014

Greene, D.J., Williams, A.C., Koller, J.M., Schlaggar, B.L., Black, K.J., 2017. Brain structure in pediatric Tourette syndrome. Mol. Psychiatry 22, 972–980. doi:10.1038/mp.2016.194

Greicius, M.D., Supekar, K., Menon, V., Dougherty, R.F., 2009. Resting-state functional connectivity reflects structural connectivity in the default mode network. Cereb. Cortex 19, 72–78. doi:10.1093/cercor/bhn059

Gu, S., Satterthwaite, T.D., Medaglia, J.D., Yang, M., Gur, R.E., Gur, R.C., Bassett, D.S., 2015. Emergence of system roles in normative neurodevelopment. Proc. Natl. Acad. Sci. 112, 13681–13686. doi:10.1073/pnas.1502829112

Guillery, R.W., 1995. Anatomical evidence concerning the role of the thalamus in corticocortical communication: a brief review. J. Anat. 187 (Pt 3, 583–592.

Gusnard, D.A., Raichle, M.E., 2001. Searching for a baseline: functional imaging and the resting human brain. Nat. Rev. Neurosci. 2, 685–694. doi:10.1038/35094500

Hardy, J., Selkoe, D.J., 2002. The amyloid hypothesis of Alzheimer's disease: Progress and problems on the road to therapeutics. Science (80-.). doi:10.1126/science.1072994

Hocke, K., Kämpfer, N., 2009. Gap filling and noise reduction of unevenly sampled data by means of the Lomb-Scargle periodogram. Atmos. Chem. Phys. 9, 4197–4206. doi:10.5194/acp-9-4197-2009

Honey, C.J., Kotter, R., Breakspear, M., Sporns, O., 2007. Network structure of cerebral cortex shapes functional connectivity on multiple time scales. Pnas 104, 10240–10245. doi:10.1073/pnas.0701519104

Hwang, K., Bertolero, M.A., Liu, W.B., D'Esposito, M., 2017. The Human Thalamus Is an Integrative Hub for Functional Brain Networks. J. Neurosci. 37, 5594–5607. doi:10.1523/JNEUROSCI.0067-17.2017

Ji, J.L., Spronk, M., Kulkarni, K., Repovš, G., Anticevic, A., Cole, M.W., 2018. Mapping the human brain's cortical-subcortical functional network organization. Neuroimage. doi:10.1016/j.neuroimage.2018.10.006

Jones, E.G., 1985. The Thalamus, 1st ed. Springer.

Kaas, J.H., 2012. Evolution of columns, modules, and domains in the neocortex of primates. Proc. Natl. Acad. Sci. 109, 10655–10660. doi:10.1073/pnas.1201892109

Kahn, I., Andrews-Hanna, J.R., Vincent, J.L., Snyder, A.Z., Buckner, R.L., 2008. Distinct Cortical Anatomy Linked to Subregions of the Medial Temporal Lobe Revealed by Intrinsic Functional Connectivity. J. Neurophysiol. 100, 129–139. doi:10.1152/jn.00077.2008

Kim, D.-J., Kent, J.S., Bolbecker, A.R., Sporns, O., Cheng, H., Newman, S.D., Puce, A., O'Donnell, B.F., Hetrick, W.P., 2014. Disrupted Modular Architecture of Cerebellum in Schizophrenia: A Graph Theoretic Analysis. Schizophr. Bull. 40, 1216–1226. doi:10.1093/schbul/sbu059

Kiritani, T., Wickersham, I.R., Seung, H.S., Shepherd, G.M.G., 2012. Hierarchical Connectivity and Connection-Specific Dynamics in the Corticospinal-Corticostriatal Microcircuit in Mouse Motor Cortex. J. Neurosci. 32, 4992–5001. doi:10.1523/JNEUROSCI.4759-11.2012

Laumann, T.O., Gordon, E.M., Adeyemo, B., Snyder, A.Z., Joo, S.J., Chen, M.-Y., Gilmore, A.W., McDermott, K.B., Nelson, S.M., Dosenbach, N.U.F., Schlaggar, B.L., Mumford, J.A., Poldrack, R.A., Petersen, S.E., 2015. Functional System and Areal Organization of a Highly Sampled Individual Human Brain. Neuron 1–14. doi:10.1016/j.neuron.2015.06.037

Laumann, T.O., Snyder, A.Z., Mitra, A., Gordon, E.M., Gratton, C., Adeyemo, B., Gilmore, A.W., Nelson, S.M., Berg, J.J., Greene, D.J., McCarthy, J.E., Tagliazucchi, E., Laufs, H., Schlaggar, B.L., Dosenbach, N.U.F., Petersen, S.E., 2016. On the Stability of BOLD fMRI Correlations. Cereb. Cortex 1–14. doi:10.1093/cercor/bhw265

Marek, S., Siegel, J.S., Gordon, E.M., Raut, R. V., Gratton, C., Newbold, D.J., Ortega, M., Laumann, T.O., Miller, D.B., Zheng, A., Lopez, K.C., Berg, J.J., Coalson, R.S., Nguyen, A.L., Dierker, D., Van, A.N., Hoyt, C.R., McDermott, K.B., Norris, S.A., Shimony, J.S., Snyder, A.Z., Nelson, S.M., Barch, D.M., Schlaggar, B.L., Raichle, M.E., Petersen, S.E., Greene, D.J., Dosenbach, N.U.F., 2018. Spatial and Temporal Organization of the Individual Human Cerebellum. Neuron Sneak Peek. doi:10.2139/ssrn.3188429

Miezin, F.M., Maccotta, L., Ollinger, J.M., Petersen, S.E., Buckner, R.L., 2000. Characterizing the hemodynamic response: Effects of presentation rate, sampling procedure, and the possibility of ordering brain activity based on relative timing. Neuroimage 11, 735–759. doi:10.1006/nimg.2000.0568

Moser, M.B., Moser, E.I., 1998. Functional differentiation in the hippocampus. Hippocampus. doi:10.1002/(SICI)1098-1063(1998)8:6<608::AID-HIPO3>3.0.CO;2-7

Nelson, S.M., Cohen, A.L., Power, J.D., Wig, G.S., Miezin, F.M., Wheeler, M.E., Velanova, K., Donaldson, D.I., Phillips, J.S., Schlaggar, B.L., Petersen, S.E., 2010. A parcellation scheme for human left lateral parietal cortex. Neuron 67, 156–170. doi:10.1016/j.neuron.2010.05.025

Neta, M., Schlaggar, B.L., Petersen, S.E., 2014. Separable responses to error, ambiguity, and reaction time in cingulo-opercular task control regions. Neuroimage 99, 59–68. doi:10.1016/j.neuroimage.2014.05.053

Nielsen, A.N., Greene, D.J., Gratton, C., Dosenbach, N.U.F., Petersen, S.E., Schlaggar, B.L., 2018. Evaluating the Prediction of Brain Maturity From Functional Connectivity After Motion Artifact Denoising. Cereb. Cortex 1–15. doi:10.1093/cercor/bhy117

Ojemann, J.G., Akbudak, E., Snyder, A.Z., McKinstry, R.C., Raichle, M.E., Conturo, T.E., 1997. Anatomic localization and quantitative analysis of gradient refocused echo-planar fMRI susceptibility artifacts. Neuroimage 6, 156–167. doi:10.1006/nimg.1997.0289

Patriat, R., Molloy, E.K., Birn, R.M., 2015. Using Edge Voxel Information to Improve Motion Regression for rs-fMRI Connectivity Studies. Brain Connect. 5, 582–595. doi:10.1089/brain.2014.0321

Petersen, S.E., Sporns, O., 2015. Brain Networks and Cognitive Architectures. Neuron 88, 207–219. doi:10.1016/j.neuron.2015.09.027

Phelps, E.A., 2006. Emotion and Cognition: Insights from Studies of the Human Amygdala. Annu. Rev. Psychol. 57, 27–53. doi:10.1146/annurev.psych.56.091103.070234

Poldrack, R.A., Laumann, T.O., Koyejo, O., Gregory, B., Hover, A., Chen, M.Y., Gorgolewski, K.J., Luci, J., Joo, S.J., Boyd, R.L., Hunicke-Smith, S., Simpson, Z.B., Caven, T., Sochat, V., Shine, J.M., Gordon, E., Snyder, A.Z., Adeyemo, B., Petersen, S.E., Glahn, D.C., Mckay, D.R., Curran, J.E., Göring, H.H.H., Carless, M.A., Blangero, J., Dougherty, R., Leemans, A., Handwerker, D.A., Frick, L., Marcotte, E.M., Mumford, J.A., 2015. Long-term neural and physiological phenotyping of a single human. Nat. Commun. 6. doi:10.1038/ncomms9885

Power, J., Schlaggar, B., Lessov-Schlaggar, C., Petersen, S., 2013. Evidence for hubs in human functional brain networks. Neuron 79, 798–813. doi:10.1016/j.neuron.2013.07.035

Power, J.D., Cohen, A.L., Nelson, S.M., Wig, G.S., Barnes, K.A., Church, J.A., Vogel, A.C., Laumann, T.O., Miezin, F.M., Schlaggar, B.L., Petersen, S.E., 2011. Functional Network Organization of the Human Brain. Neuron 72, 665–678. doi:10.1016/j.neuron.2011.09.006

Power, J.D., Mitra, A., Laumann, T.O., Snyder, A.Z., Schlaggar, B.L., Petersen, S.E., 2014. Methods to detect, characterize, and remove motion artifact in resting state fMRI. Neuroimage 84, 320–341. doi:10.1016/j.neuroimage.2013.08.048

Power, J.D., Plitt, M., Gotts, S.J., Kundu, P., Voon, V., Bandettini, P.A., Martin, A., 2018. Ridding fMRI data of motion-related influences: Removal of signals with distinct spatial and physical bases in multiecho data. Proc. Natl. Acad. Sci. 201720985. doi:10.1073/pnas.1720985115

Rajput, D.R., 1993. Accuracy of clinical diagnosis of idiopathic Parkinson's disease. J. Neurol. Neurosurg. Psychiatry. doi:10.1136/jnnp.56.8.938

Rosvall, M., Bergstrom, C.T., 2008. Maps of random walks on complex networks reveal community structure. Proc. Natl. Acad. Sci. U. S. A. 105, 1118–1123. doi:10.1073/pnas.0706851105

Roy, A.K., Shehzad, Z., Margulies, D.S., Kelly, a. M.C., Uddin, L.Q., Gotimer, K., Biswal, B.B., Castellanos, F.X., Milham, M.P., 2009. Functional connectivity of the human amygdala using resting state fMRI. Neuroimage 45, 614–626. doi:10.1016/j.neuroimage.2008.11.030

Rudolph, M.D., Miranda-Domínguez, O., Cohen, A.O., Breiner, K., Steinberg, L., Bonnie, R.J., Scott, E.S., Taylor-Thompson, K., Chein, J., Fettich, K.C., Richeson, J.A., Dellarco, D. V., Galván, A., Casey, B.J., Fair, D.A., 2017. At risk of being risky: The relationship between “brain age” under emotional states and risk preference. Dev. Cogn. Neurosci. 24, 93–106. doi:10.1016/j.dcn.2017.01.010

Satterthwaite, T.D., Wolf, D.H., Loughead, J., Ruparel, K., Elliott, M.A., Hakonarson, H., Gur, R.C., Gur, R.E., 2012. Impact of in-scanner head motion on multiple measures of functional connectivity: Relevance for studies of neurodevelopment in youth. Neuroimage 60, 623–632. doi:10.1016/j.neuroimage.2011.12.063

Schaefer, A., Kong, R., Gordon, E.M., Laumann, T.O., Zuo, X.-N., Holmes, A.J., Eickhoff, S.B., Yeo, B.T.T., 2017. Local-Global Parcellation of the Human Cerebral Cortex from Intrinsic Functional Connectivity MRI. Cereb. Cortex 1–20. doi:10.1093/cercor/bhx179

Schmahmann, J.D., 2004. Disorders of the cerebellum: ataxia, dysmetria of thought, and the cerebellar cognitive affective syndrome. J. Neuropsychiatry Clin. Neurosci. 16, 367–378. doi:10.1176/appi.neuropsych.16.3.367

Seeley, W.W., Crawford, R.K., Zhou, J., Miller, B.L., Greicius, M.D., 2009. Neurodegenerative Diseases Target Large-Scale Human Brain Networks. Neuron 62, 42–52. doi:10.1016/j.neuron.2009.03.024

Sheffield, J.M., Repovs, G., Harms, M.P., Carter, C.S., Gold, J.M., MacDonald, A.W., Daniel Ragland, J., Silverstein, S.M., Godwin, D., Barch, D.M., 2015. Fronto-parietal and cingulo-opercular network integrity and cognition in health and schizophrenia. Neuropsychologia 73, 82–93. doi:10.1016/j.neuropsychologia.2015.05.006

Siebert, M., Markowitsch, H.J., Bartel, P., 2003. Amygdala, affect and cognition: Evidence from 10 patients with Urbach-Wiethe disease. Brain 126, 2627–2637. doi:10.1093/brain/awg271

Siegel, J.S., Mitra, A., Laumann, T.O., Seitzman, B.A., Raichle, M., Corbetta, M., Snyder, A.Z., 2017. Data quality influences observed links between functional

connectivity and behavior. Cereb. Cortex 27, 4492–4502. doi:10.1093/cercor/bhw253

Siegel, J.S., Seitzman, B.A., Ramsey, L.E., Ortega, M., Gordon, E.M., Dosenbach, N.U.F., Petersen, S.E., Shulman, G.L., Corbetta, M., 2018. Re-emergence of modular brain networks in stroke recovery. Cortex 101, 44–59. doi:10.1016/j.cortex.2017.12.019

Smith, S.M., Jenkinson, M., Woolrich, M.W., Beckmann, C.F., Behrens, T.E.J., Johansen-Berg, H., Bannister, P.R., De Luca, M., Drobnjak, I., Flitney, D.E., Niazy, R.K., Saunders, J., Vickers, J., Zhang, Y., De Stefano, N., Brady, J.M., Matthews, P.M., 2004. Advances in functional and structural MR image analysis and implementation as FSL, in: NeuroImage. doi:10.1016/j.neuroimage.2004.07.051

Snyder, A.Z., Raichle, M.E., 2012. A brief history of the resting state: The Washington University perspective. Neuroimage. doi:10.1016/j.neuroimage.2012.01.044

Sorg, C., Riedl, V., Mühlau, M., Calhoun, V.D., Eichele, T., Läer, L., Drzezga, A., Förstl, H., Kurz, A., Zimmer, C., Wohlschläger, A.M., 2007. Selective changes of resting-state networks in individuals at risk for Alzheimer's disease. Proc. Natl. Acad. Sci. U. S. A. 104, 18760–18765. doi:10.1073/pnas.0708803104

Sporns, O., 2011. Networks of the Brain. MIT Press.

Sporns, O., Chialvo, D.R., Kaiser, M., Hilgetag, C.C., 2004. Organization, development and function of complex brain networks. Trends Cogn. Sci. 8, 418–425. doi:10.1016/j.tics.2004.07.008

Strick, P.L., Dum, R.P., Fiez, J.A., 2009. Cerebellum and nonmotor function. Annu. Rev. Neurosci. 32, 413–434. doi:10.1146/annurev.neuro.31.060407.125606

Talairach, J., Tournoux, P., 1988. Co-planar stereotaxic atlas of the human brain, 1988. Theime, Stuttgart, Ger. 270, 132. doi:10.1016/0303-8467(89)90128-5

Triantafyllou, C., Hoge, R.D., Krueger, G., Wiggins, C.J., Potthast, A., Wiggins, G.C., Wald, L.L., 2005. Comparison of physiological noise at 1.5 T, 3 T and 7 T and optimization of fMRI acquisition parameters. Neuroimage 26, 243–250. doi:10.1016/j.neuroimage.2005.01.007

Tulving, E., Markowitsch, H.J., 1998. Episodic and declarative memory: role of the hippocampus. Hippocampus 8, 198–204. doi:10.1002/(sici)1098-1063(1998)8:3%3C198::aid-hipo2%3E3.0.co;2-g

Van den Heuvel, M.P., Sporns, O., 2011. Rich-Club Organization of the Human Connectome. J. Neurosci. 31, 15775–15786. doi:10.1523/JNEUROSCI.3539-11.2011

Van Der Werf, Y.D., Witter, M.P., Uylings, H.B.M., Jolles, J., 2000. Neuropsychology of infarctions in the thalamus: A review. Neuropsychologia. doi:10.1016/S0028-3932(99)00104-9

Van Essen, D.C., Ugurbil, K., Auerbach, E., Barch, D., Behrens, T.E.J., Bucholz, R., Chang, A., Chen, L., Corbetta, M., Curtiss, S.W., Della Penna, S., Feinberg, D., Glasser, M.F., Harel, N., Heath, A.C., Larson-Prior, L., Marcus, D., Michalareas, G., Moeller, S., Oostenveld, R., Petersen, S.E., Prior, F., Schlaggar, B.L., Smith, S.M., Snyder, A.Z., Xu, J., Yacoub, E., 2012. The Human Connectome Project: A data acquisition perspective. Neuroimage 62, 2222–2231. doi:10.1016/j.neuroimage.2012.02.018

Vonsattel, J.-P., Myers, R.H., Stevens, T.J., Ferrante, R.J., Bird, E.D., Richardson, E.P., 1985. Neuropathological Classification of Huntington's Disease. J. Neuropathol. Exp. Neurol. 44, 559–577. doi:10.1097/00005072-198511000-00003

Wig, G.S., Laumann, T.O., Petersen, S.E., 2013. An approach for parcellating human cortical areas using resting-state correlations. Neuroimage 93, 276–291. doi:10.1016/j.neuroimage.2013.07.035

Wisse, L.E.M., Biessels, G.J., Geerlings, M.I., 2014. A critical appraisal of the hippocampal subfield segmentation package in FreeSurfer. Front. Aging Neurosci. 6. doi:10.3389/fnagi.2014.00261

Woolsey, T.A., Hanaway, J., Gado, M.H., 2008. The brain atlas: A visual guide to the human central nervous system (3rd ed.)., The brain atlas: A visual guide to the human central nervous system (3rd ed.).

Yan, C.-G., Craddock, R.C., He, Y., Milham, M.P., 2013. Addressing head motion dependencies for small-world topologies in functional connectomics. Front. Hum. Neurosci. 7. doi:10.3389/fnhum.2013.00910

Yeo, B.T.T., Krienen, F.M., Sepulcre, J., Sabuncu, M.R., Lashkari, D., Hollinshead, M., Roffman, Joshua L. Smoller, J.W., Zöllei, L., Polimeni, J.R., Fischl, B., Liu, H., Buckner, R.L., 2011. The organization of the human cerebral cortex estimated by intrinsic functional connectivity. J. Neurophysiol. 106, 1125–1165.

Zanto, T.P., Gazzaley, A., 2013. Fronto-parietal network: Flexible hub of cognitive control. Trends Cogn. Sci. doi:10.1016/j.tics.2013.10.001

Zhang, D., Snyder, A.Z., Fox, M.D., Sansbury, M.W., Shimony, J.S., Raichle, M.E., 2008. Intrinsic functional relations between human cerebral cortex and thalamus. J. Neurophysiol. 100, 1740–1748. doi:10.1152/jn.90463.2008

Zhang, D., Snyder, A.Z., Shimony, J.S., Fox, M.D., Raichle, M.E., 2010. Noninvasive functional and structural connectivity mapping of the human thalamocortical system. Cereb. Cortex 20, 1187–1194. doi:10.1093/cercor/bhp182

Supplemental Figures

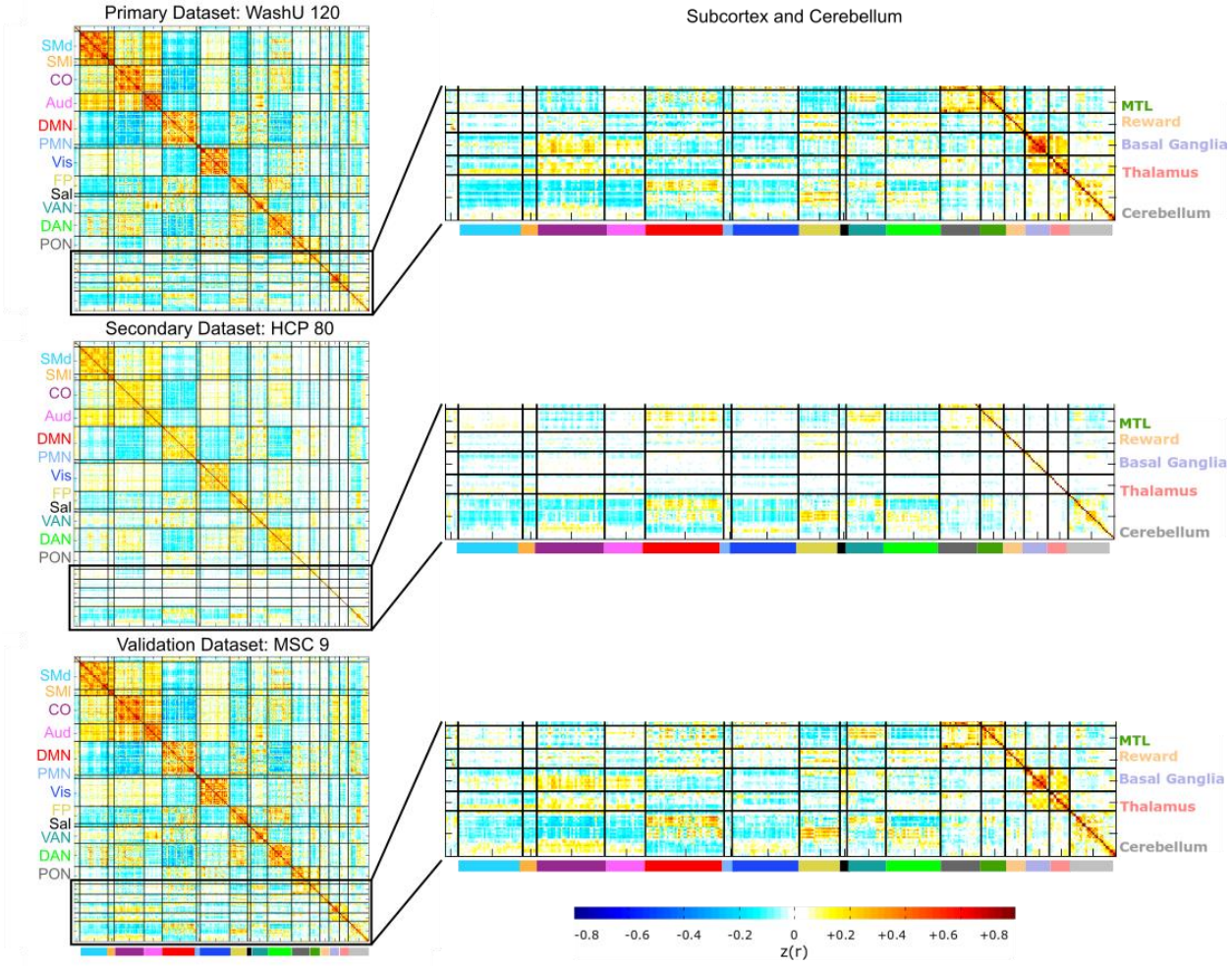

SI Figure 1: Correlation matrices for ROI Set 2. The center of each surface-based parcel from Gordon and Laumann et al., 2016 (*Cerebral Cortex*) was projected into volume space and combined with the new ROIs presented in this work to create ROI Set 2. The mean BOLD timeseries from all voxels within each ROI was extracted. The correlation matrices for each dataset are displayed, and zoomed-in portions of the matrix corresponding to the new ROIs are on the right.

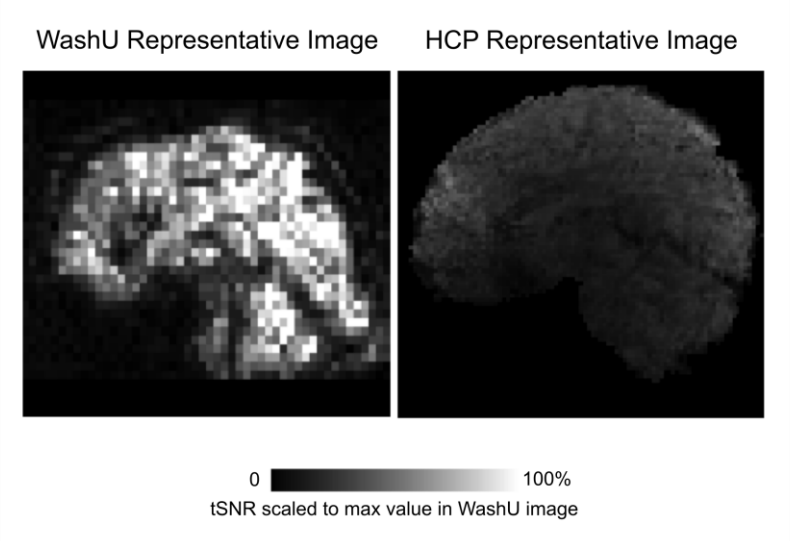

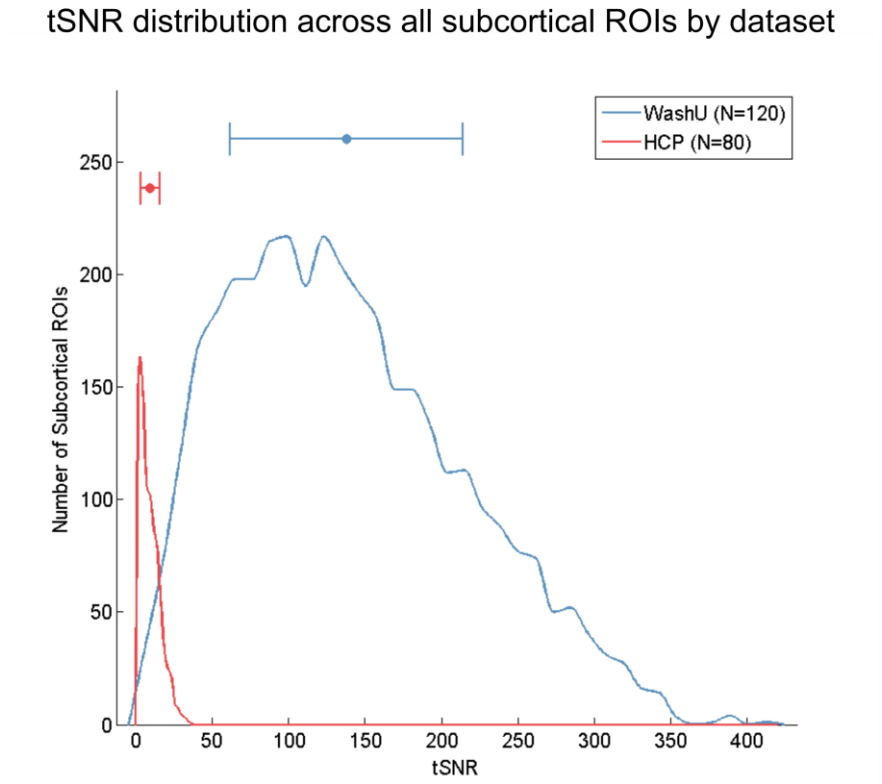

SI Figure 2: Poor temporal Signal-to-Noise Ration (tSNR) in the subcortex of Human Connectome Project data. Similar to previously published studies, we found that there was poor tSNR in the subcortex of HCP data. Representative images of tSNR (mean divided by standard deviation of the BOLD timeseries at each voxel) are displayed for an individual from the primary dataset (WashU 120) and from the HCP dataset (top). The images are scaled to the maximum tSNR value in the WashU image. The distributions on the bottom represent tSNR for all subcortical ROIs across each individual in each dataset. The distribution for HCP (red) is significantly worse than the primary dataset (mean +/- std = 9.63 +/- 6.48 for HCP; 137.79 +/- 76.22 for WashU).

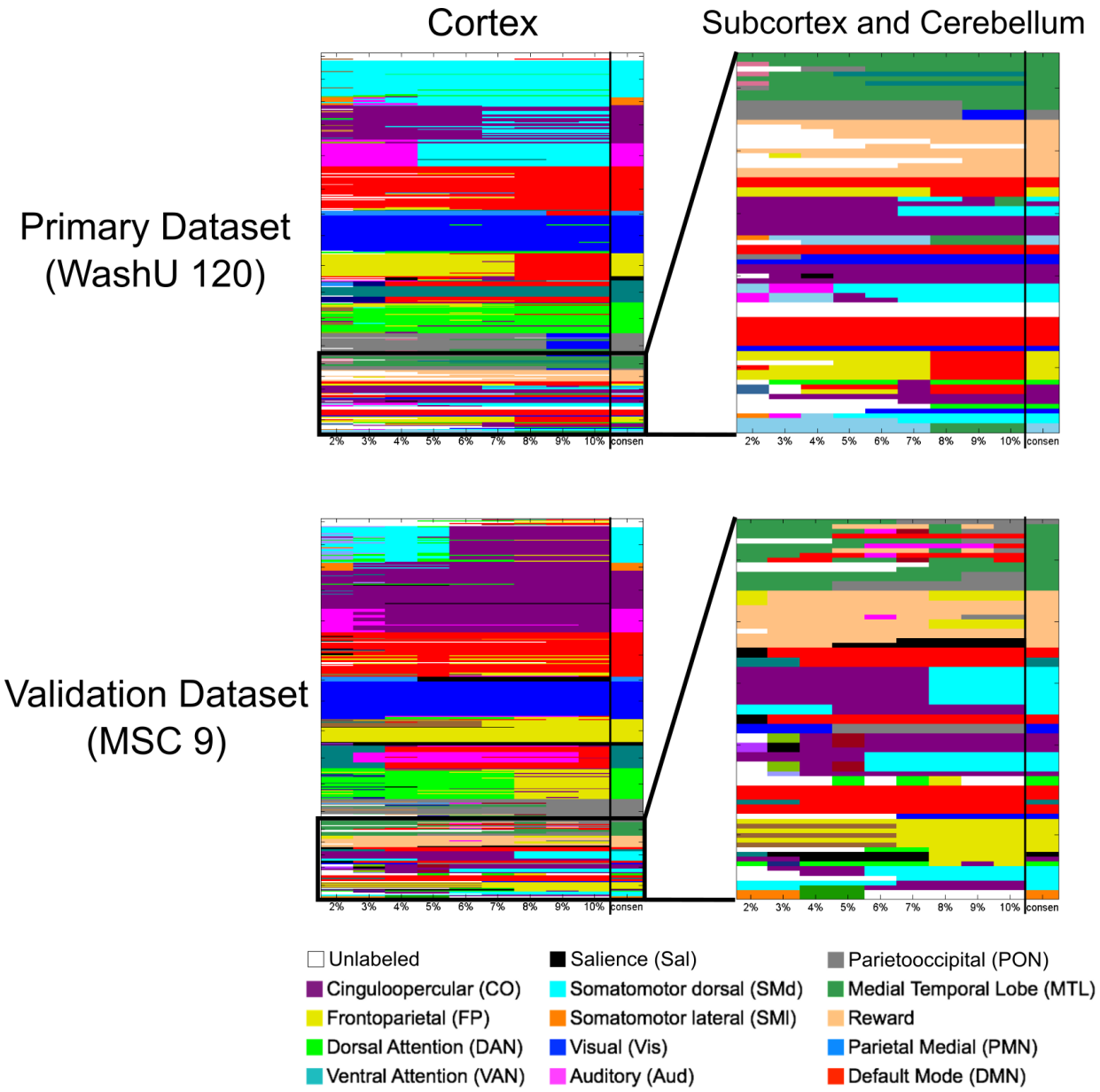

SI Figure 3: InfoMap-defined functional network community assignments for ROI Set 2. The functional network communities detected via InfoMap are displayed for the primary (WashU 120; top row) and validation (MSC; bottom row) datasets. The results were very similar to those shown in the main text, and there was good agreement between the two datasets. The primary difference is the presence of the Parietal Occipital Network in the cortex (gray), which was not observed with ROI Set 1.

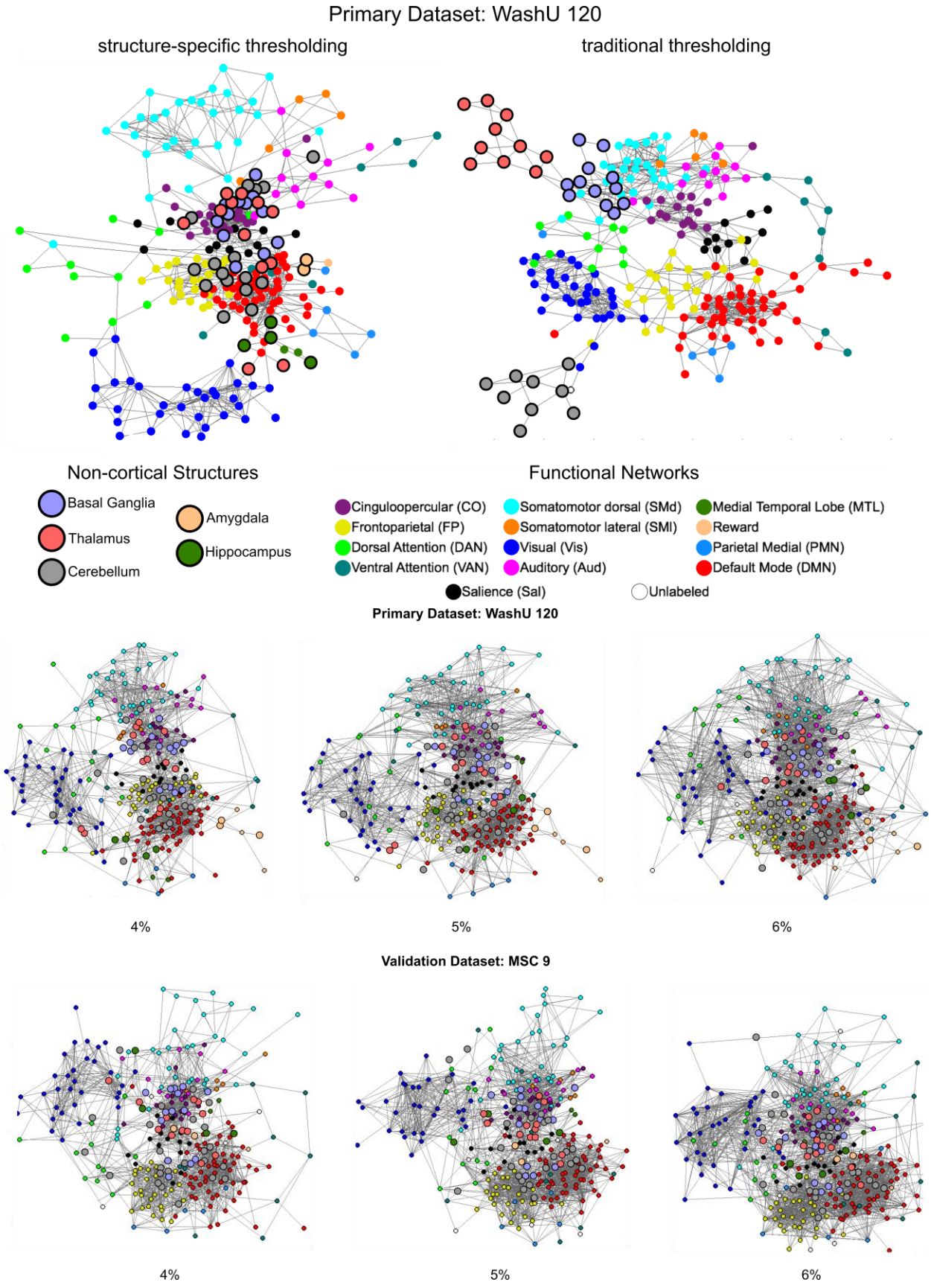

SI Figure 4: Spring-embedded graphs at other tested edge densities. The top portion of the figure shows the difference between structure-specific edge density thresholding and traditional thresholding (uniform across the matrix). The basal ganglia, thalamus, and cerebellum segregate into their own network communities when traditional thresholding is used (top right graph). Spring-embedded graphs for other structure-specific edge density thresholds are displayed in the bottom portion of the figure for the primary and validation datasets. The non-cortical ROIs (larger, bold outlines) distribute throughout each graph, integrating with known functional networks.